University of Nairobi

Faculty of Engineering

Department of Electrical and Information Engineering

Impact of Increasing Active Power Output with Reduced Excitation on Synchronous Generator Transient Stability: A Case Study of Kenya's Olkaria IV Geothermal Turbine Uprate

PIUS KIPCHUMBA KIBET

F56/67600/2013

BSc. (EEE) – JKUAT, 2012

Thesis submitted for the Degree of Master of Science in Electrical & Electronic Engineering in the Department of Electrical & Information Engineering of the University of Nairobi

April 2023

DECLARATION

PIUS KIPCHUMBA KIBET

F56/67600/2013

SIGNATURE   DATE: **April 2023**

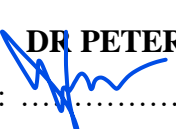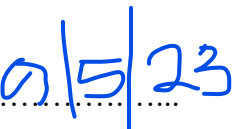This Thesis is submitted with our approval as University Supervisors:

<u>SUPERVISORS:</u>

PROF H. A. OUMA

SIGNATURE: ……………………… DATE: 09/05/2023

Department of Electrical and Information Engineering

University of Nairobi

DR PETER MUSAU

SIGNATURE: ……………………. DATE: 0/5/23

Department of Electrical, Electronics, and Information Engineering

South Eastern Kenya University

DECLARATION OF ORIGINALITY

KIBET PIUS KIPCHUMBA

REG. NO: F56/67600/2013

Faculty of Engineering

Department of Electrical & Information Engineering

Master of Science in Electrical and Electronic Engineering

Impact of Increasing Active Power Output with Reduced Excitation on Synchronous Generator Transient Stability: A Case Study of Kenya's Olkaria IV Geothermal Turbine Uprate

1. I understand what plagiarism is and I am aware of the university policy in this regard.
2. I declare that this Thesis is my original work and has not been submitted elsewhere for examination, award of a degree, or publication. Where other people's work or my own work has been used, this has properly been acknowledged and referenced in accordance with the University of Nairobi's requirements.
3. I have not sought or used the services of any professional agencies to produce this work.
4. I have not allowed and shall not allow anyone to copy my work with the intention of passing it off as his/her own work.
5. I understand that any false claim in respect of this work shall result in disciplinary action, in accordance with University's anti-plagiarism policy.

Signature:

Date: **April 2023**

ii

ACKNOWLEDGEMENT

I would like to take this golden opportunity to express my appreciation and gratitude to the Department of Electrical and Information Engineering at the University of Nairobi for offering me a chance and for being a pillar in the development of this thesis, which has paved the way to the completion of my MSc work. I would like to thank Dr. P. Musau and Prof. H. A. Ouma for their great supervision and for being a constant source of support, guidance, and inspiration during the period of my thesis. I would also like to thank my employer, KenGen PLC, for its provision of material support and financial muscle. Lastly, I want to appreciate and thank my wife and children, as well as my parents, for the moral support they have given me towards this achievement.

TABLE OF CONTENTS

LIST OF FIGURES

LIST OF TABLES

LIST OF SYMBOLS, ABBREVIATIONS, NOMENCLATURE

AU – additional units

AVR – automatic voltage regulator

bara – bar absolute

CCA – critical clearing angle

CT – clearing time

CCT – critical clearing time

δ – load angle

E – internal voltage

EAC – equal area criterion

EM – Euler Method

EPRA – Energy and Petroleum Regulatory Authority

ETAP – electrical transient and analysis program

Fig - Figure

GPP – Geothermal Power Plant

H – Moment of inertia constant

HPP – Hydro Power Plant

HVAC – High Voltage Alternating Current

HVDC – High Voltage Direct Current

I – current

IEEE – Institute of Electrical and Electronics Engineers

J – moment of inertia

KE – kinetic energy

KenGen – Kenya Electricity Generating Company

KPLC – Kenya Power and Lighting Company

MEM – modified Euler method

MW - MegaWatt

MVA - MegaVolt-Ampere

MVAr - MegaVolt-Ampere reactive

LTWP – Lake Turkana Wind Power

P - active power

PE – potential energy

PEBS – potential energy boundary surfaces

p.f. - power factor

p.u – per unit

PSS – power system stability

Q - reactive power

R – Resistance

RKM – Runge – Kutta Method

S - Apparent power

SEP – stable equilibrium point

SG – synchronous generator

STATCOM - Static Synchronous Compensator

SVC – Static Var Compensator

s - seconds/laplace operator

SG – Synchronous Generator

SIMB - Single Machine Infinite Bus

T – Torque

TEF – Transient Energy Function

t - time

t/h - ton per hour

V – Volt

WHDS – Wellheads

ω – Generator Speed in radians

X - Reactance

Z - Impedance

ABSTRACT

Power system stability refers to the ability of synchronous machines that are connected to a power system to remain stable in operation after being subjected to any form of disturbance. The stability of a power system depends on the initial operating conditions determined by parameters such as mechanical input power P_m to the generator from the turbine, electrical or air gap power P_e, which is a function of machine voltage behind the synchronous reactance (proportional to the excitation current) E_f, generator synchronous reactance X_s, and load angle δ. Power system stability issues are mainly classified into two categories: steady-state and transient. Steady-state deals with small perturbations that can be linearized; after a perturbation, the system returns to its original stable operating point. Transient stability is concerned with the impact of a large disturbance, such as the loss of significant loads or generation, an electrical fault, or the sudden outage of a transmission line. During a transient condition, the system exhibits nonlinearization characteristics and resumes a new stable operating point. This thesis presents an equal area criterion (EAC) as a solution method to problems of transient stability for a single-machine system. However, other transient stability methods are described in this work. The ETAP software is used to model and simulate transient stability. Olkaria IV geothermal power plant, owned by Kenya Electricity Generating Company PLC (KenGen), is taken as a case study. The power plant has two machines, each with an installed capacity of 75 MW. The company plans to uprate the turbine from 75 MW to 83 MW due to the availability of sufficient steam resources as well as its strategic plan of increasing the generated power to 2500 MW by 2025. An increase in active power will affect stability parameters such as the critical rotor angle and critical clearing time. The analyzed results from EAC, which is a graphical method, are compared with the modified Euler method (MEM), which is a numerical method. The comparison is done to ensure and confirm the correctness. The thesis proved that an increase in the synchronous generator's active power increases the critical clearing angle and reduces the critical clearing time. The outcome of this research will be useful to the generating company when additional generation is planned. It is recommended to consider other ways of maintaining reactive power and voltage in the network through the installation of equipment such as static compensators (STATCOM) or capacitor banks.

Key Words – Power System Stability (PSS), Transient Stability (TS), Equal Area Criterion (EAC)

CHAPTER 1: INTRODUCTION

1.1   Background

A typical power system comprises generation, transmission, distribution, and customer loads. The demand for electrical energy is increasing day by day; this has necessitated power sectors worldwide to move towards market liberation and competition [1]. Modern power systems are becoming more complex as a result of interconnection, the installation of large generating units, and transmission lines [2]. Power system stability is the capability of an electric power system to recover by developing forces that are greater than or equal to disturbance forces to ensure that the equilibrium state is maintained [3]. Factors that are considered when analyzing stability include loading in the network, the nature of the fault and its location, fault clearing time, changes in the rotor angle position, and the machines' inertia [4]. Stability studies are aimed at understanding how synchronous machines behave when a disturbance occurs in a power system [5].

Power system analyses are mainly in two categories: steady-state stability and transient stability. Steady-state stability is when a power system returns to its original steady-state condition of operation after a small disturbance. In a power system operating in a steady-state condition and experiencing a change in parameters that can be linearized and expressed using algebraic equations, a small disturbance is said to have occurred [6]. Transient stability deals with system behavior after a large disturbance [7]. The main aim of transient stability is to find the values of rotor angles that preserve the integrity of the power system by maintaining synchronism. The integrity of the system is preserved only if the entire power system remains intact without tripping of generators or loads in the system, except for those disconnected by isolation of the faulted elements or intentionally tripped to preserve the continuity of operation of the rest of the power system [8].

Transient stability is regarded as one of the constraints when it comes to the planning and maintenance of power system operations as far as security is concerned [4]. Other forms of stability are normally encountered in the power system, such as voltage stability, dynamic stability, and frequency stability; these will be explained in the coming sections. The stability limit refers to the maximum power transferred in a network between the sending station (source) and receiving station (load) before synchronism is lost (9). If the balance between the generator's electromagnetic

and mechanical torques is lost following a system disturbance, rotor oscillations will occur [7]. Power system stability is a measure of synchronism in terms of rotor angle [10]. Stability problems in electrical power networks revolve around the evaluation of the mechanical and electrical dynamic equations for the synchronous machines [11].

This thesis is a case study of a geothermal power plant in Kenya located at Olkaria IV with machines of 75 MW that are planned for an uprate to increase the active power output to 83 MW. The machine will also undergo a change in the power factor (p.f.) from 0.85 lagging to 0.95 lagging, and apparent power will be maintained at 88 MVA. This will be achieved by modifying the turbine to produce more mechanical power and limiting the excitation current. These changes have the potential to alter the stability of the machine. Therefore, there is a need to carry out a study to establish the impact of these changes.

1.2   Problem statement

The lack of stability studies on the impact of Olkaria IV steam turbine uprate is the main concern. KenGen PLC is planning to increase the generator's active power from 75 MW at a power factor of 0.85 lagging and reactive power of 46 MVARs to 83 MW at a power factor of 0.95 lagging and reactive power of 27 MVARs. The apparent rating of the generator will be maintained at 88 MVA. A study is necessary because it gives information about the stability condition of the power system for secure operation. The absence of stability information can lead to the generator being operated outside its stability limits. Operating machines without a clear guide on stability limits increases the chances of loss of synchronism when a system disturbance occurs, hence leading to rotor oscillations. Speed oscillations in machines increase wear and tear, can cause resonance and blade failures in turbines, and can trip the generator on the loss of synchronism protection. Tripping of a large generator can trigger cascade-tripping of other generators in the grid and cause a national blackout.

1.3   Objectives

Objectives are classified as main and specific.

1.3.1 Main objective

Analyse the impact of increased generator active power and reducing the reactive power on transient stability of Olkaria IV generator.

1.3.2 Specific objectives

i)   Calculate the steady-state operating point of the existing machine at 75 MW.

ii) Calculate the new steady-state operating point of the uprated turbine at 83 MW.

iii) Model, simulate, and analyze the generator's transient behavior when subjected to a disturbance.

iv) Validate the analytic results from the transient stability.

1.4   Research questions

i)   What is the steady-state operating point of the existing machine at 75 MW?

ii) What is the new steady-state operating point of the uprated machine at 83MW?

iii) How do the generator dynamic parameters behave during power system disturbance?

iv) Do the research results correlate with the known accepted values?

1.5   Justification

This research was conducted at Kenya Electricity Generating Company PLC (KenGen) premises. KenGen PLC is a public company; its ownership is 70% owned by the government of Kenya and 30% by the public. Its core business is the generation of electricity from various sources of energy, such as hydro, geothermal, diesel, and wind. Besides KenGen, there are independent power producers (IPPs) licensed by the government to generate electric power and sell it to the Kenya Power and Lighting Company (KPLC). Currently, the electricity market share for KenGen PLC is about 62%, according to [12].

Due to the abundant availability of geothermal steam resources of about 10,000 MW in Kenya, the government is shifting focus to intensifying the expansion of geothermal power generation to meet the growing energy demand, which is projected to be 4251 MW by 2030 [12]. Because of its renewable nature, being clean, and having a lower cost compared to fuel (fossil) energy,

geothermal energy becomes an option. Technically, geothermal machines are contributing more to the stability of the system because they have a higher inertia constant as compared to hydro machines. By carrying out stability studies, the generating companies will use the research outcome for planning purposes when it comes to increasing generation. This is done to avoid compromising the stability of the system. Hence, this study will mitigate the stability problem by recommending the optimum operating parameters for the Olkaria IV generator after the turbine uprate. Also, the data and models derived will be useful for future expansion into geothermal power generation.

1.6   Scope

This research is limited to the transient stability analysis of the Olkaria IV generator using the equal area criterion method. Hydro, wind, engine, and gas turbine-driven generators are excluded from this work. The analysis involves modeling, simulation, analysis, and validation of the results. The EAC results are compared to the modified Euler method to ascertain their correctness. Live testing on the actual system was not done for safety, system security, and operational reasons.

1.7   Thesis organization

The thesis comprises five chapters as follows.

Chapter one describes the background, essence, and significance of power system stability, the problem statement, objectives, research questions, and the scope of work.

Chapter two gives the literature on power system stability, explains the commonly encountered forms of disturbances in a typical power system, and discusses previous related studies, research gaps, modeling techniques, power transfer, and swing equations.

Chapter three outlines the methodology employed to achieve the objectives, describes the available solution methods to the transient stability problem, and explains the choice behind the employed method.

Chapter four contains the models, simulation results, and analyses of the results.

Chapter five has the thesis conclusions and the recommendations based on the findings.

CHAPTER 2: LITERATURE REVIEW
2.1 Basics of power system stability

Power system stability (PSS) is defined as the ability to regain a state of operating equilibrium after being subjected to any form of system disturbance [13]. It is about maintaining equilibrium between the two opposing forces i.e. mechanical and electrical. If the forces holding the machines in synchronism with the rest power system are sufficient to neutralize the disturbing forces, the system is regarded as stable.

The stability issues are concerned with the response of a synchronous generator to a system disturbance. Stability studies are commonly carried out by power utility companies to ensure that the dynamic performance of the power system is proper [6]. These studies are usually performed when a new generator or transmission line is planned to be connected to the power system [5]. For stable operations of the power system, the following two conditions should be made for synchronous generators; synchronism of the rotor should be kept and generated voltage waveforms should be sinusoidal with equal frequencies. During power system disturbance, the two conditions are breached and instability can occur [14]. Stability is achieved in synchronous generators when there is an equilibrium between the two opposite-acting forces.

Stability issues are majorly categorized into two forms; steady-state and transient stability. Steady-state stability is the ability of the power system to maintain synchronism following a small disturbance. Dynamic stability is much similar to the steady-state, the only difference is that it lasts longer and takes care of the effects of automatic control devices such as the generator's automatic voltage regulators and turbine governors.

Transient stability is the ability of the power system to resume a new stable equilibrium state following a large disturbance such as the loss of a large generator, load, or tripping of a transmission line [5]. When a power system is subjected to disturbances, its stability is determined by the magnitude and nature of the disturbance and initial operating condition. The disturbance may be small or large. Small disturbances consist of changes in the system loads, occurring continually and randomly. Power systems should be designed to adjust to this constantly changing environment and withstand disturbances of a severe nature, such as a short circuit on a transmission

line or a loss of a large generator connected to the power system, for better performance. Generally, the system must be operated reliably and securely to ensure quality power to the customers. Otherwise, if the system is unstable, a runaway or a rundown situation can occur, such as an uncontrollable increase or decrease in rotor angle or a fall in system voltage. Instability in the power system can cause cascade tripping of generators leading to a complete or partial blackout.

2.1.1 Power system stability classifications

Power system stability classification enables complex problems to be solved using effective and convenient methods. The objective is to ease the analysis of power system problems.
The approach is to identify factors contributing to instability and find the appropriate ways of improving it. Factors considered when classifying a power system include; the physical nature of the instability, the magnitude of the disturbance, elements such as processes, devices, and time, and the method of analysis [8]

Fig. 2.1 [15] illustrates the classification of power system stability. Rotor and voltage stability are major classes, and each constitutes two sub-classes, large signal, and small-signal stability. Rotor angle stability and voltage stability are affected by an electrical fault in the power system while frequency stability is related to load or generation change in the power system.
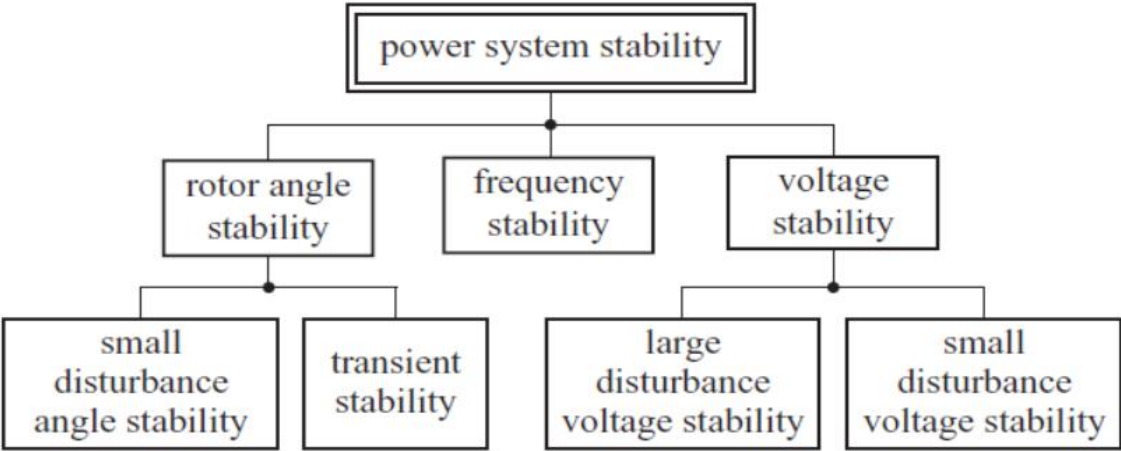
Fig 2.1: Classifications of power system stability

2.1.2   Rotor angle stability

Rotor angle stability is the ability of a synchronous generator to remain in synchronism with the power system when subjected to a physical disturbance.

The term rotor angle is very crucial in transient stability studies; it has both physical significance and an electrical interpretation. It is defined as the spatial angle between the rotor magnetic field and the revolving air-gap field, neglecting stator leakage flux. A rotor angle can either be positive or negative; when it is positive, the rotor field is said to be leading the air-gap field and power flows into the power system, or simply the machine is in generation mode. In synchronous machines, the conversion of energy can be reversed, and at times, the rotor angle can assume a negative value. This means power flows from the power system to the mechanical load; when this occurs, the machine is said to be motoring [11]. See Fig. 2.2 [9] for the illustration the concept of the rotor angle. The symbols; WS, θ_e, and δ denote the revolving air-gap field, rotor angular position, and rotor angle, respectively, of a synchronous generator.
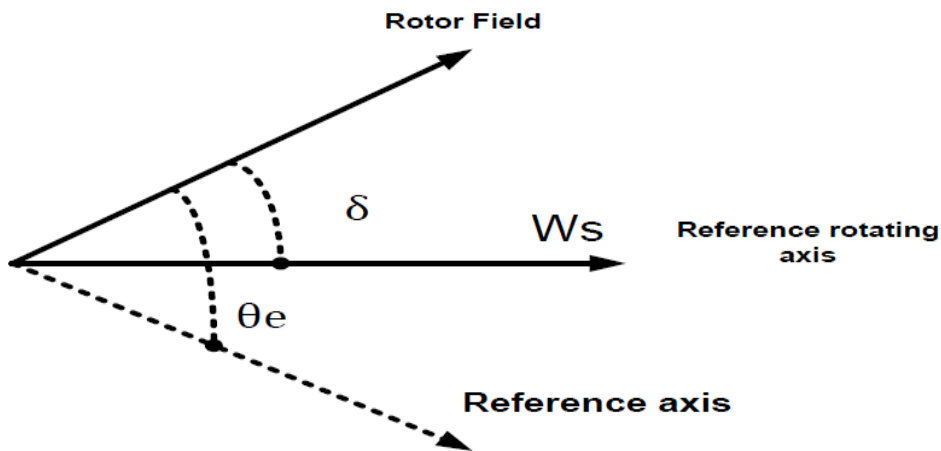
Fig. 2.2: Phasor diagram of a SG showing a rotor angle

The power output of synchronous generators varies as their rotor angles oscillate periodically. When synchronism is lost in a synchronous generator, its rotor runs at a higher or lower speed than

the nominal speed. Under steady-state conditions, electromagnetic and mechanical torques are equal, and if the system is disturbed, the equilibrium is lost, thus causing the rotor to accelerate or decelerate. Synchronism can be maintained by the restoration of forces on the collapsing side [8] When a system disturbance occurs, there is a change in electrical toque ΔT_e that can be resolved into two components by (2.1).

$$\Delta T_e = (T_s \Delta\delta) + (T_D \Delta\omega) \tag{2.1}$$

where $T_s \Delta\delta$ denotes a torque change component in phase with the rotor angle displacement $\Delta\delta$, referred to as the synchronizing torque coefficient, $T_D \Delta\omega$ denotes a torque change component in phase with the speed deviation $\Delta\omega$, referred to as the damping torque coefficient. System stability depends on the existence of the two components of torque on the synchronous generator. Insufficient synchronizing torque may cause instability through periodic drifting in the rotor angle position, while insufficient damping torque may cause rotor oscillation.

2.1.3   Transient stability

Transient stability is the ability of a synchronous generator to remain in synchronism with the power system when subjected to a severe disturbance [8]. Following a severe disturbance, the rotor angle of the synchronous machine changes as a result of the rotor acceleration [7].

Transient stability uses non-linear models for analysis [16]. This type of stability is a function of the initial operating state of the system and the magnitude of the disturbance. The disturbance causes a transition of the generator's operating point from one equilibrium point to another equilibrium point that is stable.

The transient stability limit defines the maximum electrical power transferred before the system becomes unstable in the event of a severe disturbance [9].

Power system usually experiences different degrees of severity of disturbances. However, the system should be designed to withstand contingencies without becoming unstable. These contingencies include short circuits such as phase-to-ground, phase-to-phase-to-ground, and a bolted three-phase. These faults are always assumed to be occurring on a transmission line, but they can also occur on a bus or transformer. The protection system should clear faults within the shortest time possible by initiating the tripping of appropriate breakers to isolate the faulted

sections of the power system. In cases of transmission line faults, high-speed re-closures are always recommended. By doing this, stability can be greatly improved [8].

2.1.4   Steady-state stability

Steady-state stability is the ability of a synchronous generator to remain in synchronism when subjected to minimal system disturbance [8]. Disturbances of that nature normally occur continually and randomly in the system because of its inherent characteristics, which impose changes on loads and generation. This type of stability is also known as a small signal and is solved by the linear method to determine if the system is stable or not [6].

During normal system operations, customers connect loads randomly, and turbine governors respond to these load changes by adjusting generation, leading to small oscillations or instability. The steady-state stability limit defines the maximum electrical power transferred before the system becomes unstable after increasing the load gradually, under the condition of steady-state [9].

The instability that arises comes in two forms, one leading to a steady increase in rotor angle due to insufficient synchronizing torque and the other leading to rotor angle oscillations with increasing amplitude due to insufficient damping torque. The system naturally responds to these small disturbances, with its performance determined by factors such as the initial operating point, the transmission system strength, and the performance characteristics of the generator controls (excitation and governing systems). In the case of a synchronous generator connected to a large power system without an automatic voltage regulator, instability normally arises because of insufficient synchronizing power or torque [9].

2.1.5   Voltage stability

Voltage stability is defined as the ability of a synchronous generator to maintain a steady, acceptable voltage at its terminal under normal operating conditions and during a disturbance. The power system experiences voltage instability following an increase in load demand or change in system operating condition, causing a progressive and uncontrollable fall or rise in voltage levels on the bus and generator terminals. Causes of voltage instability are the inadequacy of power systems to meet the demand for reactive power, thus leading to a voltage drop occurring when

active and reactive power flow through an inductive circuit such as a highly loaded transmission line and transformers [8].

2.1.6 Frequency stability

Frequency stability is the ability of a power system to maintain a steady frequency within allowable boundaries [8]. When a severe system disturbance occurs, there will be a big difference between the load and generation. The imbalance should be restored by the turbine governor and automatic generation control (AGC) within the appropriate time to maintain power quality.

2.1.7 Dynamic stability

The term dynamic stability simply refers to introducing a means of stability to a naturally unstable system through the implementation of automatic control devices such as turbine governors and generator automatic voltage regulators. In most cases, prevalent in studying small-signal disturbances of the order ranging from 10 to 30 sec time durations [17].

2.1.8 Factors affecting transient stability

The following are the factors that affect transient stability as presented by Kundur [8].

a) Generator loading: the heavily loaded generator is susceptible to instabilities.

b) Proximity of the fault location and generator output: the nearer the fault location, the greater the instability.

c) The duration of the fault before it is cleared: A shorter fault clearance time improves stability.

d) Reactance of the transmission line: a small reactance improves stability.

e) Generator reactance or a short circuit ratio (SCR): SCR is a reciprocal of the synchronous reactance; the higher the value, the higher the stability.

f) Generator inertia, H: the higher the value of H, the greater the stability of the system.

g) Generator voltage behind reactance: higher values improve stability.

h) System bus voltage: a larger magnitude improves stability.

2.2 Previous studies

Gross stated in his work [11] that the power system began as early as 1945, and this was the time the equal area criterion was encountered. Since then, the complexity of the power systems has consistently advanced, and this has led to the emergence of computer-based systems to solve transient stability problems. A few examples of transient stability studies carried out in the past are described in this thesis.

In a study by Sharma [2], titled "Transient stability analysis of power systems using MATLAB," the author modeled the system with an IEEE 9 bus using the MATLAB program and simulated a three-phase fault at the bus with distinct fault clearing times. Sharma's work involved a multi-machine model consisting of three generators, lines, buses, and other system components. He used the admittance method and Kron's reduction formula to eliminate all other buses except the generator ones. This study compared the simulation results from MATLAB with those from PSPICE and found them to be more accurate.

Abbas [3] analyzed transient stability using the load angle method for a multimachine system and recommended the use of machine learning mechanisms in evaluating the transient stability for greater accuracy of the results. This was after carrying out a case study of a power substation in Sudan and modeling the system using the ETAP program.

"Effects of power system parameters on transient stability studies," by Agber *et al* [4], describes how factors such as the location of a fault, load increment, damping factor of the machine, time to clear a fault, and the machine's synchronous speed can influence transient stability. The study used the numerical integration method to arrive at a solution to stability problems for multimachine systems. The authors used the modified Euler method in computing the power angles and speeds for the machines and concluded that the closer the fault location, the smaller the critical clearing time.

An article by Himadri *et al*. [14] analyzed transient stability using the direct method and the time domain method by modeling a multimachine system consisting of two machines and nine buses and simulating it using the power system analysis toolbox (PSAT), a tool running in MATLAB.

Himadri concluded that the time domain method is time-consuming when used to analyze the transient stability and supported the use of direct methods based on the computation of energies.

A study by Sutter and Maleche [18] titled "Analysis of power system transient stability due to increased integration of geothermal power" emphasized the need for carrying out an assessment to establish the impact of increased injection of geothermal generation into the Kenyan grid on system stability. According to this study, geothermal power was expected to increase to 5530 MW by 2030. The authors showed, through mathematical expression, that the machine inertia constant H determines the stability of the machine when evaluated with the time a synchronous machine takes to come to a standstill when mechanical power is removed. As stated in this work, geothermal machines have a higher value of H than hydro machines and therefore contribute to the stability of the power system.

Transient stability using step-by-step and equal area criteria [19] by Al Marhoon was one of the most interesting articles that used the direct method to evaluate the transient of a multi-machine power system. Al Marhoon presented a detailed mathematical model of Lyapunov in his work. Although it did not indicate explicitly how it is used to solve practical power system problems, it is a source of valuable material when it comes to understanding the Lyapunov method as a solution to transient stability analysis. The study used the IEEE 39 bus system to simulate a multimachine system and the Power System Analysis Toolbox (PSAT) to analyze the system. Al Marhoon pointed out that the choice of PSAT as the simulation tool was due to its availability and capability of performing power flows and numerical integration.

Injection of more generation into the power system causes changes in the stability of the system, as stated by Lopez [20] in his work "modeling and analyzing stability at El Salvador geothermal power plants around Berlin". This work used MATLAB and Simulink software to build and simulate the system model and considered the contributions of control elements such as the turbine governor and generator excitation system. The study was more about dynamic stability analysis than transient stability analysis because it incorporated control and damping elements, which are normally characterized by finite time constants and thus their responses extend beyond ten seconds.

A classical system model can be improved by taking the effect of damping into consideration when analyzing the transient stability response, as mentioned by Padhi [21] in his article titled "Representation of transient stability for power system dynamics using numerical integration method and dynamics". Padhi stated that bus voltages, power flows in the lines, and the performance of the protection system are additional items of importance on top of the basic stability elements. Padhi's work considered the contribution of damping from the d-axis and q-axis amortisseurs during the simulation. Padhi further simulated the system for a duration of ten seconds with damping included, but this contradicts a book by Kundur [8] that limits transient stability studies to 3 to 5 seconds for smaller systems and 10 seconds for larger systems. Traditionally, damping and control elements have time constants that may exceed 10 seconds and should be considered for steady-state analysis, as indicated by Rao [9].

A few previous studies on transient stability are summarized in Table 2.1.

Table 2.1: Summary of the literature review

NO.	Author	Title	Method of analysis
1	Sharma [2]	Transient Stability Analysis of Power System Using MATLAB	Numerical
2	Abbas [3]	Power System Transient Stability Case Study: A Power Sub-Station Plant in Sudan	Load angle
3	Agber [4]	Effects of Power System Parameters on Transient Stability Studies	Not stated
4	Himadri et al [14]	Transient Stability Analysis of Synchronous Generator in Power System	Numerical and direct
5	Sutter and Maleche [18].	Analysis of Power System Transient Stability Due to Increased Integration of Geothermal Power	Not stated
6	Al Marhoon [19].	Practical Method of Power System Transient Stability and Security	Equal area criterion and step-by-step.
7	Alonso [20].	Modeling and Stability Analysis of Berlin Geothermal Power Plant (CGB) in El Salvador.	Not stated
8	Padhi [21]	Representation of Transient Stability for Power System Dynamics Using Numerical Integration Method and Damping	Numerical
9	P. Kibet	Impact of Increasing Active Power Output with Reduced Excitation on Synchronous Generator Transient Stability: A Case Study of Kenya's Olkaria IV Geothermal Turbine Uprate	Direct/Equal Area Criterion

2.3 Research gaps

A study by Sutter and Maleche [18] pointed out the need for carrying out an assessment to establish the impact of increased injection of geothermal generation into the Kenyan grid on stability. The authors clearly brought out that increased injection of geothermal machines into the power system would improve the stability of the power system due to a higher value of the inertia constant. Also, Agber *et al.* [4] stated that load increment affects the transient stability of a system. This thesis is an enhancement of Sutter and Maleche [18] and Agber *et al.* [4] through a case study seeking to establish the correlation between the machine's active power, reactive power, and transient stability. This was carried out by analyzing transient stability using the equal area criterion (EAC).

2.4 System modelling

Modeling is the process of emulating a real-world situation. A model illustrates a framework concept that describes a system and may be regarded as an emulator of an actual process or system or a replica of a physical system or situational state. Modeling is the representation of a factual state or a state of reality. The commonly available models applicable in engineering are mathematical, electrical, and software models. Mathematical models are normally used to describe systems using variable names. Variables values may be simply anything of a kind, such as an integer or real number, Boolean values, a string of characters, and so on [22]. Models can be developed using the Simulink tool in MATLAB, the electrical transient and analysis program (ETAP), or any other program. Mathematical, electrical, ETAP, and Simulink models have been used predominantly in this work.

2.5 Problem formulation

This section entails the two essential equations applied in transient stability analysis including the swing equation and power transfer equation. The swing equation describes the generator rotor's dynamic behaviour when subjected to a disturbance while the power transfer equation gives a profile of electrical quantities and describes the relationship among them.

2.5.1 Power transfer equations

The power transfer equation for synchronous generators (SG) is very important in transient stability analysis. The mathematical expression of the power transfer equation for the SG is derived

by considering the quantities per phase [23]. The windings of the SG are normally configured in a star for grounding purposes. The connection to the ground ensures stability and protection for the machine. Zero-sequence currents flow to the ground, thus making the protection relays detect and trip the machine in case of a fault.

2.5.2 Power equations for a synchronous generator (sg)

Fig. 2.3 [24] shows the schematic diagram of a synchronous generator (round machine), indicating various electrical quantities.
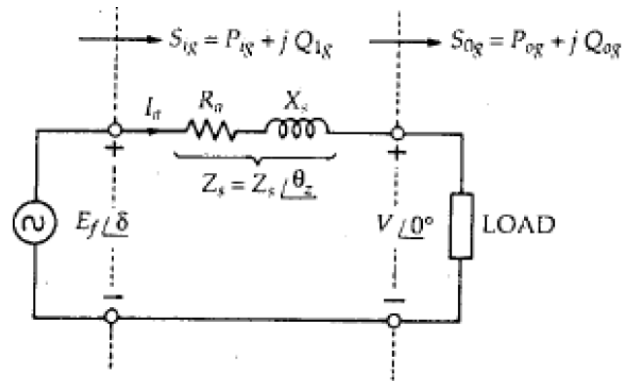
Fig. 2.3: Electrical model of a SG with a round rotor

The quantities V, E_f, I_a, Z_s, R_a, S, Q, θ_z, and δ represent terminal voltage, open circuit voltage per phase, armature or load current, impedance, armature resistance, apparent power, reactive power, power factor, and rotor, respectively. Fig. 2.4 [24] is a phasor diagram of Fig. 2.3.
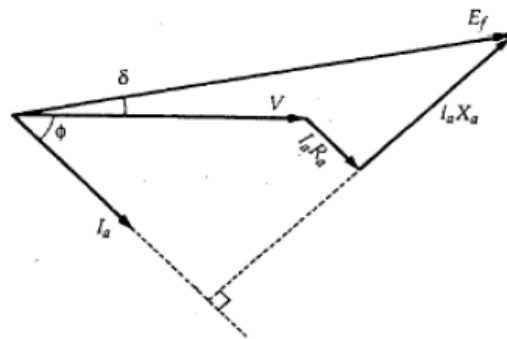
Fig. 2.4: Phasor diagram of a SG at lagging power factor

The quantity V lags E_f by an angle δ, thus

$$\mathbf{V} = V \angle 0 \tag{2.2}$$

$$\mathbf{E_f} = E_f \angle \delta \tag{2.3}$$

The impedance triangle in Fig. 2.5 [24] is a graphical representation of equation (2.4).

$$Z_s = R_a + jX_s = Z_s \angle \theta_z \tag{2.4}$$
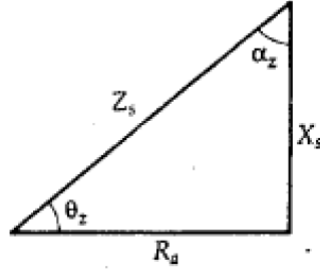
Fig. 2.5: Impedance triangle

With, $\theta_z = \tan^{-1}\frac{X_s}{R_a}$, $\propto_z = 90° - \theta_z = \tan^{-1}\frac{R_a}{X_s}$ and letting the subscripts $i,\ o,\ g$ represent input, output, generator respectively, then.

$$\mathbf{E_f} = V + Z_s \mathbf{I_a} \tag{2.5}$$

$$\mathbf{I_a} = \frac{\mathbf{E_f} - V}{Z_s} \tag{2.6}$$

Complex power output of the generator per phase (S_{og}) is computed by (2.7)

$$S_{og} = P_{og} + jQ_{og} = V\mathbf{I_a}^* \tag{2.7}$$

Substituting $\mathbf{I_a}$ in (2.7) leads to (2.8),

$$S_{og} = V\left(\frac{\mathbf{E_f} - V}{Z_s}\right)^*$$

$$= V\angle 0° \left(\frac{E_f \angle \delta - V\angle 0°}{Z_s \angle \theta_z}\right)^*$$

$$= V\angle 0° \left(\frac{E_f}{Z_s}\angle(\delta - \theta_z) - \frac{V}{Z_s}\angle - \theta_z\right)^*$$

$$= \left(\frac{VE_f}{Z_s}\angle \delta - \theta_z - \frac{V^2}{Z_s}\angle - \theta_z\right)^*$$

$$\therefore P_{og} + jQ_{og} = \frac{VE_f}{Z_s}\cos(\theta_z - \delta) + j\frac{VE_f}{Z_s}\sin(\theta_z - \delta) - \frac{V^2}{Z_s}(\cos\theta_z + j\sin\theta_z) \tag{2.8}$$

2.5.3   Real output power per phase of a SG (P_{og})

Equation (2.9) evaluates the active output power of the generator by including resistance R_a

$$P_{og} = \frac{VE_f}{Z_s}\cos(\theta_z - \delta) - \frac{V^2}{Z_s}\cos\theta_z \tag{2.9}$$

Since $\cos\theta_z = \frac{R_a}{Z_s}$, (2.9) becomes

$$P_{og} = \frac{VE_f}{Z_s}\cos(\theta_z - \delta) - \frac{V^2}{Z_s^2}R_a \qquad (2.10)$$

But $\quad \theta_z = 90° - \alpha_z$, thus (2.10) becomes

$$\therefore P_{og} = \frac{VE_f}{Z_s}\cos[90° - (\delta + \alpha_z)] - \frac{V^2}{Z_s^2}R_a \qquad (2.11)$$

Or

$$P_{og} = \frac{VE_f}{Z_s}\sin(\delta + \alpha_z) - \frac{V^2}{Z_s^2}R_a \qquad (2.12)$$

2.5.4   Reactive output power per phase of a SG (Q_{og})

Equation (2.13) evaluates the reactive output power of the generator by including synchronous impedance X_s.

$$Q_{og} = \frac{VE_f}{Z_s}\sin(\theta_z - \delta) - \frac{V^2}{Z_s}\sin\theta_z \qquad (2.13)$$

Since $\quad \sin\theta_z = \frac{X_s}{Z_s}$, then (2.13) becomes

$$Q_{og} = \frac{VE_f}{Z_s}\sin(\theta_z - \delta) - \frac{V^2}{Z_s^2}X_s \qquad (2.14)$$

But $\quad \theta_z = 90° - \alpha_z$, thus (2.14) gives

$$\therefore Q_{og} = \frac{VE_f}{Z_s}\sin[90° - (\delta + \alpha_z)] - \frac{V^2}{Z_s^2}X_s \qquad (2.15)$$

$$Q_{og} = \frac{VE_f}{Z_s}\cos(\delta + \alpha_z) - \frac{V^2}{Z_s^2}X_s \qquad (2.16)$$

2.5.5   Complex power input to a SG per phase (S_{ig})

Equation (2.17) gives a complex input power of a SG considering all the circuit parameters.

$$S_{ig} = P_{ig} + Q_{ig} = E_f I_a^* \qquad (2.17)$$

Substituting (2.3) and (2.6) in (2.7) gives

$$S_{ig} = E_f\angle\delta\left(\frac{E_f}{Z_s}\angle(\theta_z - \delta) - \frac{V}{Z_s}\angle\theta_z\right)$$

Or

$$P_{ig} + Q_{ig} = \frac{E_f^2}{Z_s} \angle \theta_z - \frac{VE_f}{Z_s} \angle (\theta_z + \delta) \tag{2.18}$$

$$\therefore P_{ig} + Q_{ig} = \frac{E_f^2}{Z_s} cos\theta_z + j\frac{E_f^2}{Z_s} sin\theta_z - \left[\frac{VE_f}{Z_s} cos(\theta_z + \delta) + j\frac{VE_f}{Z_s} sin(\theta_z + \delta)\right] \tag{2.19}$$

2.5.6   Real power input to a SG per phase (P_{ig})

The real power input to the SG transferred from the prime mover is given by (2.20).

$$P_{ig} = \frac{E_f^2}{Z_s} cos\theta_z - \frac{VE_f}{Z_s} cos(\alpha_z + \delta) \tag{2.20}$$

Since $cos\,\theta_z = \frac{R_a}{Z_s}$, then

$$P_{ig} = \frac{E_f^2}{Z_s^2} R_a - \frac{VE_f}{Z_s} cos(\theta_z + \delta) \tag{2.21}$$

But $\theta_z = 90° - \alpha_z$, thus

$$\therefore P_{ig} = \frac{E_f^2}{Z_s^2} R_a - \frac{VE_f}{Z_s} cos[90° + (\delta - \alpha_z)] \tag{2.22}$$

Or

$$P_{ig} = \frac{E_f^2}{Z_s^2} R_a + \frac{VE_f}{Z_s} sin(\delta - \alpha_z) \tag{2.23}$$

2.5.7   Reactive power input to a SG per phase (Q_{ig})

Reactive power input to the SG transferred from excitation is evaluated by (2.24).

$$Q_{ig} = \frac{E_f^2}{Z_s} sin\theta_z - \frac{VE_f}{Z_s} sin(\theta_z + \delta) \tag{2.24}$$

But $sin\,\theta_z = \frac{X_s}{Z_s}$, thus

$$\therefore Q_{ig} = \frac{E_f^2}{Z_s^2} X_s - \frac{VE_f}{Z_s} sin(\theta_z + \delta) \tag{2.25}$$

Since $\theta_z = 90° - \alpha_z$, thus

$$sin(\theta_z + \delta) = sin(90° + \delta - \alpha_z) = cos(\delta - \alpha_z)$$

$$\therefore Q_{ig} = \frac{E_f^2}{Z_s^2} X_s - \frac{VE_f}{Z_s} cos(\delta - \alpha_z) \tag{2.26}$$

2.5.8 Maximum real power output of a SG per phase $P_{og\ (max)}$

The maximum power output of the generator is achieved when

$$\frac{dP_{og}}{d\delta} = 0 \ \ and \ \ \frac{d^2P_{og}}{d\delta^2} < 0$$

Differentiating equation (2.12)

$P_{og} = \frac{VE_f}{Z_s}\sin(\delta + \alpha_z) - \frac{V}{Z_s{}^2}{}^2 R_a$ w.r.t δ and equating it to zero we get

$$\frac{d}{d\delta}\left[\frac{VE_f}{Z_s}\sin(\delta + \alpha_z) - \frac{V}{Z_s{}^2}{}^2 R_a\right] = 0 \tag{2.27}$$

Since V, E_f, Z_s and R_a are constants,

$$\frac{VE_f}{Z_s}\cos(\delta + \alpha_z) = 0 \tag{2.28}$$

Therefore, $\cos(\delta + \alpha_z) = 0$

Since $\cos 90°(2n + 1) = 0$, where n = 0, 1, 2, …, for general case, for this case, n = 0 will be used and may apply to others because cosines of angles are periodic quantities.

$\delta + \alpha_z = 90°$, and $\sin(\delta + \alpha_z) = 1$

Substituting $\sin(\delta + \alpha_z)$ in (2.12) yields,

$$P_{og\ (max)} = \frac{VE_f}{Z_s} - \frac{V}{Z_s{}^2}{}^2 R_a \tag{2.29}$$

2.5.9 Maximum power input to a SG per phase $P_{ig\ (max)}$

Condition of achieving the maximum power input to the generator is achieved if

$$\frac{dP_{ig}}{d\delta} = 0 \ \ and \ \ \frac{d^2P_{ig}}{d\delta^2} < 0$$

Differentiating   (2.20)

$P_{ig} = \frac{E_f{}^2}{Z^2{}_s}R_a + \frac{VE_f}{Z_s}\sin(\delta - \alpha_z)$ w.r.t δ and equating it to zero we get

$$\frac{d}{d\delta}\left[\frac{E_f{}^2}{Z^2{}_s}R_a + \frac{VE_f}{Z_s}\sin(\delta - \alpha_z)\right] = 0 \tag{2.30}$$

Since V, E_f, Z_s and R_a are constants,

$$\frac{VE_f}{Z_s}\cos(\delta - \alpha_z) = 0 \tag{2.31}$$

Since $\cos 90°(2n + 1) = 0$, where n = 0, 1, 2, …, for general case. For this case, n = 0 will be used and may apply to others because angles are rotating quantities.

For maximum input power to be achieved, $(\delta - \alpha_z) = 90°$, substituting this in (2.23) gives,

$$P_{ig(max)} = \frac{E_f^2}{Z_s^2} R_a + \frac{VE_f}{Z_s} \tag{2.32}$$

2.5.10 Power flow equations for a SG with armature resistance neglected

In practical polyphase synchronous machines $R_a \ll X_s$ and therefore, R_a is neglected. Neglecting armature R_a, $Z_s = X_s$, $\alpha_z = 0$. Therefore, the active and reactive input and output powers are represented by (2.33-2.37). The parameter X_s is commonly referred to as transfer reactance.

$$P_{og} = \frac{VE_f}{X_s} \sin\delta \tag{2.33}$$

$$Q_{og} = \frac{VE_f}{X_s} \cos\delta - \frac{V^2}{X_s^2} \tag{2.34}$$

$$P_{ig} = \frac{VE_f}{X_s} \sin\delta = P_{og} \tag{2.35}$$

$$Q_{ig} = \frac{E_f^2}{X_s} - \frac{VE_f}{X_s} \cos\delta \tag{2.36}$$

$$P_{og(max)} = \frac{VE_f}{X_s} = P_{ig(max)} \tag{2.37}$$

2.5.11 The swing equation

The swing equation describes the dynamic behavior of the synchronous generator during transients. It is very crucial when determining the stability of the system. The swing equation revolves around the two counter torques, mechanical and electrical. Normally, the two torques are equal; when balance is lost between the two, acceleration torques emerge, as shown by (2.38) [25].

$$T_a = T_m - T_e \tag{2.38}$$

Where T_a, T_m and T_e are the acceleration torque, mechanical torque, and electrical torque, respectively, in N.m.

Equation (2.38) can be modified by introducing the total inertia of the generator and prime mover responsible for the acceleration and deceleration, as shown by (2.39).

$$J \frac{d\omega_m}{dt} = T_a = T_m - T_e \tag{2.39}$$

Where J, ω_m, and t denote the moment of inertia of the generator and prime mover in kg.m^2, the rotor mechanical speed in rad/s, and time in seconds. Normalizing (2.39) by introducing inertia constant H, where H is the ratio of kinetic energy (watt-seconds) at nominal rated speed to machine rating in VA$_{base}$ and ω_{0m} is mechanical rated speed of the generator rad/s, H is therefore expressed as

$$H = \frac{1}{2} \frac{J \omega^2_{0m}}{VA_{base}} \tag{2.40}$$

Making J the subject of formula in (2.40),

$$J = \frac{2H}{\omega^2_{0m}} VA_{base} \tag{2.41}$$

Substituting J in (2.39)

$$\frac{2H}{\omega^2_{0m}} VA_{base} \frac{d\omega_m}{dt} = T_m - T_e \tag{2.42}$$

Rearranging (2.39) yields:

$$2H \frac{d}{dt}\left(\frac{\omega_m}{\omega_{0m}}\right) = \frac{T_m - T_e}{VA_{base}/\omega_{0m}} \tag{2.43}$$

From (2.43), it is noted that $T_{base} = VA_{base}/\omega_{0m}$

Writing (2.39) in per unit (pu)

$$2H \frac{d\bar{\omega}_r}{dt} = \bar{T}_m - \bar{T}_e \tag{2.44}$$

Also, the speed can be written in per unit form as:

$$\overline{\omega_r} = \frac{\omega_m}{\omega_{0m}} = \frac{\omega_r/Pf}{\omega_0/Pf} = \frac{\omega_r}{\omega_0} \tag{2.45}$$

Where ω_r denotes the rotor angular speed in electrical rad/s, ω_0 is the rotor nominal rated angular speed in rad/s, Pf denotes the number of rotor field poles.

Taking δ as rotor angle in electrical radians at any given time, t and its value at time t = 0 is δ_0, thus instantaneous rotor angle is written as.

$$\delta = \omega_r t - \omega_0 t + \delta_0 \tag{2.46}$$

Taking time derivative on both sides, we have:

$$\frac{d\delta}{dt} = \omega_r - \omega_0 = \Delta\omega_r \tag{2.47}$$

Differentiating again w.r.t time gives:

$$\frac{d^2\delta}{dt^2} = \frac{d\omega_r}{dt} = \frac{d(\Delta\omega_r)}{dt}$$

$$= \omega_0 \frac{d\overline{\omega_r}}{dt} = \omega_0 \frac{d(\Delta\overline{\omega_r})}{dt} \tag{2.48}$$

Substituting for $\frac{d\overline{\omega_r}}{dt}$ given by (2.48) in (2.44) gives,

$$\frac{2H}{\omega_0} \frac{d^2\delta}{dt^2} = \overline{T_m} - \overline{T_e} \tag{2.49}$$

By including a component of damping torque that is proportional to speed deviation in the (2.49) becomes:

$$\frac{2H}{\omega_0} \frac{d^2\delta}{dt^2} = \overline{T_m} - \overline{T_e} - K_D \Delta\overline{\omega_r} \tag{2.50}$$

Equation (2.50) is called the swing equation.

Where:

$$\Delta\overline{\omega_r} = \frac{\Delta\omega_r}{\omega_0} = \frac{1}{\omega_0} \frac{d\delta}{dt} \tag{2.51}$$

The symbol K_D denotes the damping factor or coefficient in pu torque/pu speed deviation.

Therefore equation (2.50) becomes:

$$\frac{2H}{\omega_0} \frac{d^2\delta}{dt^2} = \overline{T_m} - \overline{T_e} - \frac{K_D}{\omega_0} \frac{d\delta}{dt} \tag{2.52}$$

Equations (2.50) and (2.51) can be transformed into first-order differential equations as.

$$p\Delta\overline{\omega_r} = \frac{1}{2H}(\overline{T_m} - \overline{T_e} - K_D \Delta\overline{\omega_r}) \tag{2.53}$$

$$p\delta = \omega_0 \Delta\overline{\omega_r} \tag{2.54}$$

Where $\omega_0 = 2\pi f_0$ is the nominal angular speed in electrical rad/s, $\Delta\overline{\omega}_r$ denotes the speed deviation of the in p.u, p is an operator representing derivative d/dt.

2.5.12 Classical system model

In the classical approach, several assumptions are made for simplicity's sake during transient stability analysis. New technologies, such as the computerized-based approach, have improved the processes of transient stability analysis [26]. Fig. 2.6 [26] illustrates a classical model of the system for Single-Machine Infinite-Bus (SMIB). This work will apply this method.
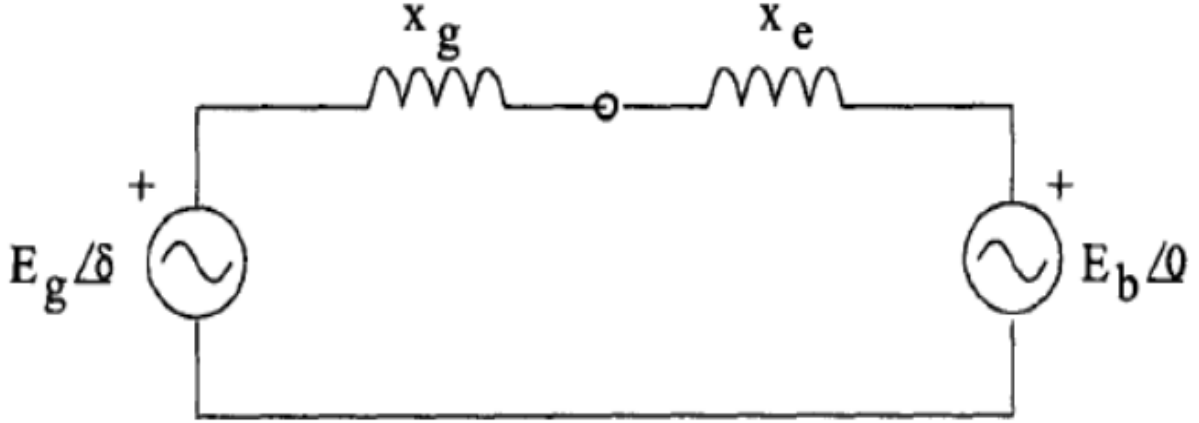
Fig. 2.6: Classical model of SMIB

Referring to the model of Fig 2.6, electrical active power output is given by (2.55)

$$P_e = \frac{E_g E_b}{X_T} \sin \delta = P_{max} \sin \delta \qquad (2.55)$$

Where P_{max} is defined as,

$$P_{max} = \frac{E_g E_b}{X_T} \qquad (2.56)$$

$X_T = X_g + X_e$, total system impedance.

Therefore, the swing equation is rewritten as

$$\frac{2H}{\omega_0} \frac{d^2 \delta}{dt^2} = P_m - P_{max} \sin \delta \qquad (2.57)$$

Where P_e, P_m, P_{max}, E_g, E_b, x_g, x_e, and δ denote the electrical power, mechanical power, maximum air-gap power, internal voltage behind the synchronous reactance (function of machine excitation), system (bus) voltage, generator synchronous reactance, system reactance, and rotor (load) angle, respectively.

The expression in (2.57) has neglected the damping because its value is very small and associated with a large time constant when it comes to the transient stability analysis, which requires only a short time, say one to two seconds. Damping is normally achieved through power system stabilizers and is only considered when analyzing steady-state stability, as mentioned in [26]. Also, the excitation control system is assumed to be in manual mode or with slow-acting automatic voltage regulators; the generator has no rotor damper connections; and there is no change in the mechanical input power to the generator. These assumptions are only valid in the classical model.

2.6 Chapter conclusion

Chapter two gives the literature on power system stability, describes in detail the swing and power transfer equations, and explains a few previous related studies.

CHAPTER 3: METHODOLOGY

This chapter involves the collection of system data from sources such as the manufacturer's manual, equipment nameplates, datasheets, and real-time measurements. After the collection of data, the system was modeled and simulated using the ETAP software. The simulation considered three conditions: pre-fault, fault, and post-fault. The results from the simulation were analyzed using the equal area criterion (EAC) and modified Euler methods (MEM). The analyzed results were compared to verify the correctness of EAC. Fig. 3.1 is a flow chart illustrating the methodology applied in this thesis.
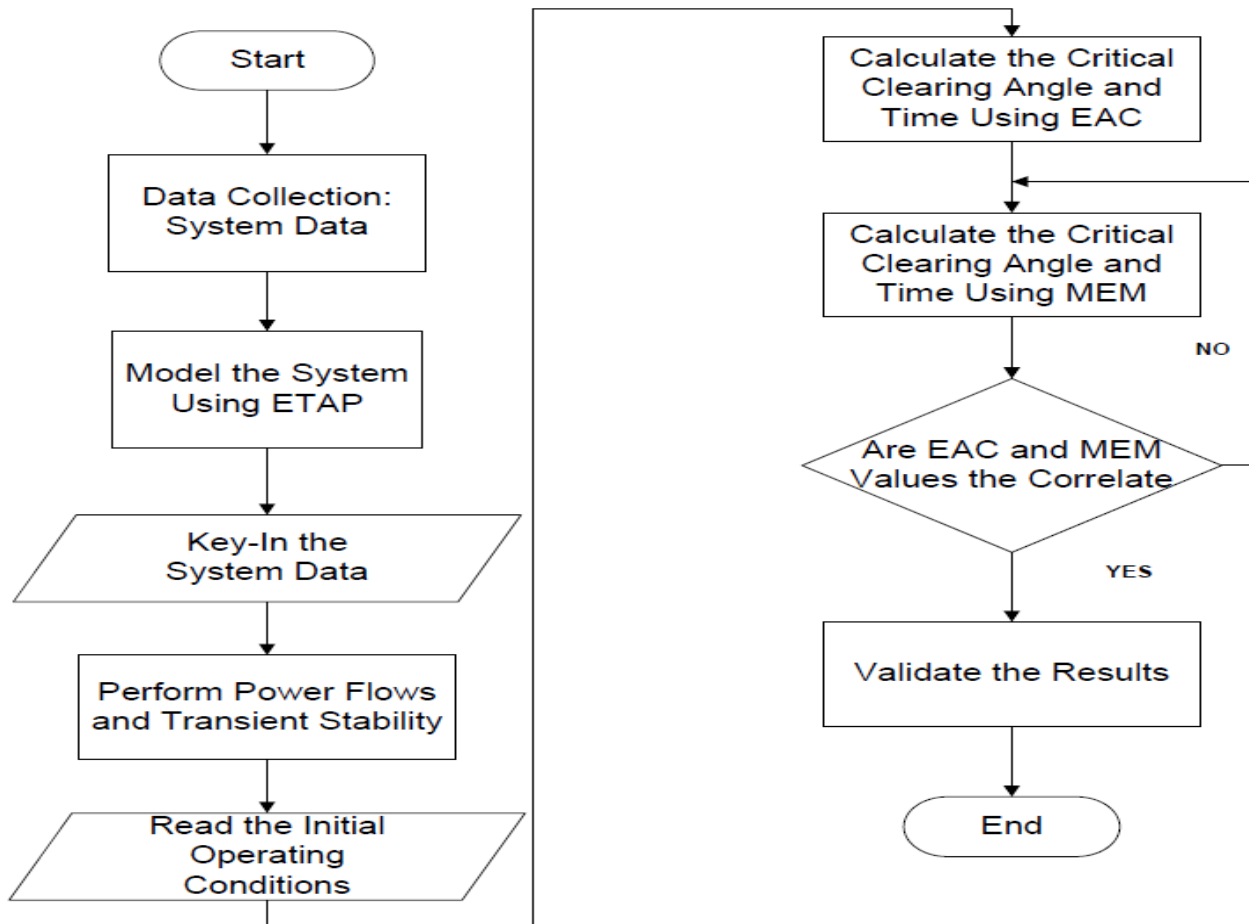
Fig. 3.1: Flowchart of the methodology

Methods of analyzing transient stability are mainly classified into two categories: numerical methods and direct methods. These methods will be described in this chapter in detail.

3.1 Numerical methods

Numerical integration methods give approximate solutions to non-linear differential equations such as a swing equation. These methods come with computer-based algorithms that offer solutions to numerical integration. The simplest one is Euler's method; this method has the least accuracy when compared to all other numerical methods [5]. Digital simulation techniques are becoming the norm when it comes to solving power system transient problems [19]. Numerical methods are further classified into explicit and implicit methods.

3.1.1 Explicit methods

Made of the Euler method, the modified Euler method, and the Runge-Kutta method.

3.1.1.1 The Euler method

The Euler method (EM) [27] is only applicable to the first-order differential equation of the form

$$\frac{dx}{dt} = f(x, t) \tag{3.1}$$

As shown in Fig. 3.2 [27], EM is depicted by the plot of t against x. The curve represents the system dynamics, with x corresponding to the rotor angle. In transient stability analysis, a solution is sought to determine the time response of the rotor angle.
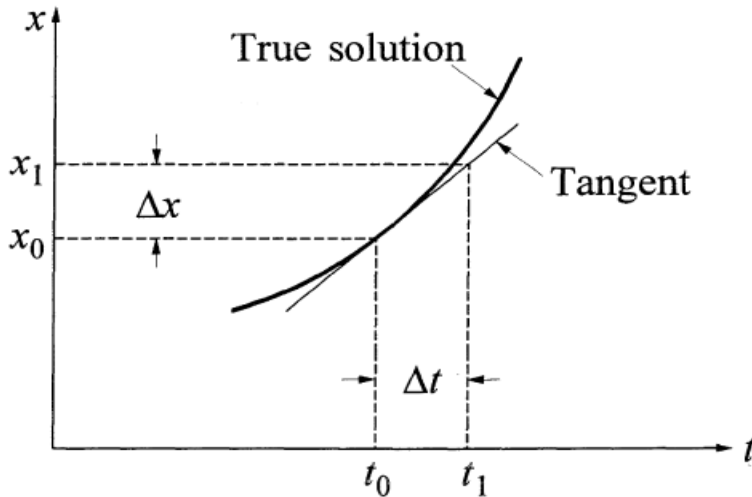
Fig. 3.2: Graphical representation of the EM

From the graph, at $x = x_0$, and $t = t_0$, and the tangent of the curve is

$$\left.\frac{dx}{dt}\right|_{x=x_0} = f(x_0, t_0) \tag{3.2}$$

26

And then

$$\Delta x = \Delta t. \frac{dx}{dt}\bigg|_{x=x_0} \tag{3.3}$$

Therefore, the value of x at $t = t_1 = t_0 + \Delta t$ is computed as

$$x_1 = x_0 + \Delta x = x_0 + \Delta t. \frac{dx}{dt}\bigg|_{x=x_0} \tag{3.4}$$

The method uses a Taylor series expansion that considers only up to two terms of x around the point (x_0, t_0)

$$x_1 = x_0 + \Delta t(\dot{x}_0) + \frac{\Delta t^2}{2!}(\ddot{x}_0) + \frac{\Delta t^3}{3!}(\dddot{x}_0) + \cdots \tag{3.5}$$

Similarly, x_2 is computed as

$$x_2 = x_1 + \Delta t. \frac{dx}{dt}\bigg|_{x=x_1} \tag{3.6}$$

And the complete approximation is

$$x_2 = x_1 + \Delta t(\dot{x}_1) + \frac{\Delta t^2}{2!}(\ddot{x}_1) + \frac{\Delta t^3}{3!}(\dddot{x}_1) + \cdots \tag{3.7}$$

3.1.1.2 The modified Euler method

The accuracy of the standard Euler method in (3.5) and (3.7) is limited because it assumes the derivative at the beginning is the same throughout the interval [26]. This shortcoming is overcome by the modified Euler method (MEM), which averages the two derivatives at both ends using two steps of prediction and correction.

Predictor: Uses derivative at the beginning of the step to predict the value at the end of the step.

$$x^p_1 = x_0 + \Delta t. \frac{dx}{dt}\bigg|_{x=x_0} \tag{3.8}$$

Corrector: Predicted value x^p_1, is used to obtain the end step derivative. Finally, the two derivatives at the start and end are averaged.

$$x^c_1 = x_0 + \frac{1}{2}\left(\frac{dx}{dt}\bigg|_{x=x_0} + \frac{dx}{dt}\bigg|_{x=x^p_1}\right)\Delta t \tag{3.9}$$

.

Applying the Euler method to solve the swing equation [5]

$$\frac{H}{\pi f_0} \frac{d^2 \delta}{dt^2} = P_m - P_e \tag{3.10}$$

Taking $\frac{H}{\pi f_0} = \frac{2H}{\omega_0}$

Rearranging (3.10) in the form

$$\frac{d^2 \delta}{dt^2} = \frac{\pi f_0}{H}(P_m - P_e \sin\delta) = \frac{\pi f_0}{H} P_a \tag{3.11}$$

The parameters, P_a and f denote the acceleration power and system frequency respectively.

The swing equation in (3.11) is decomposed into a state variable form as

$$\frac{d\delta}{dt} = \Delta\omega, \ \frac{d\Delta\omega}{dt} = \frac{\pi f_0}{H} P_a \tag{3.12}$$

Applying the MEM to (3.12)

$$\delta^p{}_1 = \delta_0 + \Delta t.\frac{d\delta}{dt}\bigg|_{\delta=\delta_0}$$

$$\Delta\omega^p{}_1 = \Delta\omega_0 + \Delta t.\frac{d\Delta\omega}{dt}\bigg|_{\Delta\omega=\Delta\omega_0}$$

The predicted values $\delta^p{}_1$ and $\Delta\omega^p{}_1$ yields the derivatives at the end of interval

$$\frac{d\delta}{dt}\bigg|_{\delta=\delta^p{}_1} = \Delta\omega^p{}_1$$

$$\frac{d\Delta\omega}{dt}\bigg|_{\Delta\omega=\Delta\omega^p{}_1} = \frac{\pi f_0}{H} P_a\bigg|_{\Delta\omega=\Delta\omega^p{}_1} \tag{3.13}$$

Then the corrected values are

$$\delta^c{}_1 = \delta_0 + \Delta t.\left(\frac{\frac{d\delta}{dt}\big|_{\delta=\delta_0} + \frac{d\delta}{dt}\big|_{\delta=\delta^p{}_1}}{2}\right)$$

$$\Delta\omega^c{}_1 = \Delta\omega_0 + \Delta t.\left(\frac{\frac{d\Delta\omega}{dt}\big|_{\Delta\omega=\Delta\omega_0} + \frac{d\Delta\omega}{dt}\big|_{\Delta\omega=\Delta\omega^p{}_1}}{2}\right) \tag{3.14}$$

The advantage of the Euler method is its simplicity, but its drawback is the numerical error introduced when ignoring the higher-order terms in the Taylor series expansion. The errors can be minimized by using reasonably small values of Δt, this value must be chosen carefully. Decreasing it too much increases computer round-off errors, and increasing it too much leads to limitations in

computing capability [5]. Fig. 3.3 [5] shows the deviation of the approximated curve from the true curve when using MEM. The MEM helps with the basics and lays the foundation for understanding more complex methods such as Runge-Kutta.
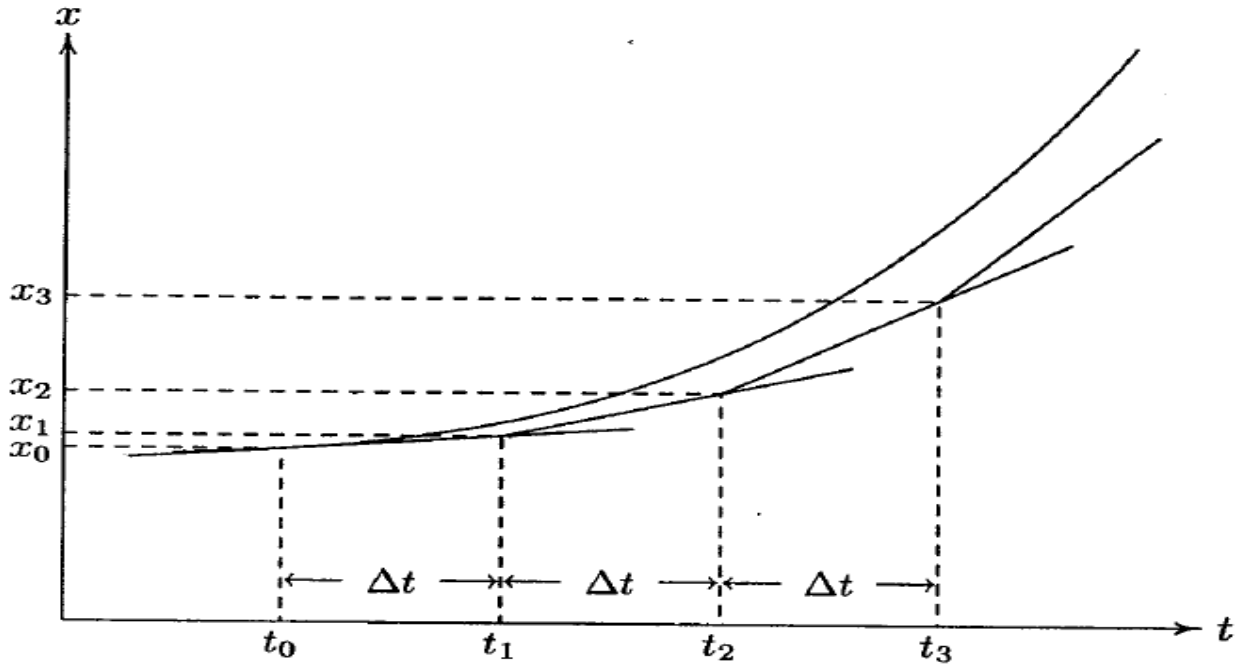
Fig. 3.3: Approximation errors in the MEM

3.1.1.3 Runge-Kutta (RK) methods

Runge-Kutta methods [27] consist of second-order and fourth-order.

a) Second order RK method

The value of x at $t = t_0 + \Delta t$ for the second RK method is

$$x_1 = x_0 + \Delta x = x_0 + \frac{k_1 + k_2}{2} \tag{3.15}$$

given $k_1 = f(x_0, t_0)\Delta t$ and $k_2 = f(x_0 + k_1, t_0 + \Delta t)\Delta t$

the general value of x at the $(n + 1)^{th}$ is

$$x_{n+1} = x_n + \frac{k_1 + k_2}{2} \tag{3.16}$$

with $k_1 = f(x_n, t_n)\Delta t$ and $k_2 = f(x_n + k_1, t_n + \Delta t)\Delta t$

The method is referred to as second-order because it takes the Taylor series expansion up to the second derivative term.

b) Fourth order RK method

Generally, x for the $(n+1)^{th}$ step is

$$x_{n+1} = x_n + \frac{1}{6}(k_1 + 2k_2 + 2k_3 + k_4)$$ (3.17)

Where $k_1 = f(x_n, t_n)\Delta t$, $\quad k_2 = f(x_n + \frac{k_1}{2}, t_n + \frac{\Delta t}{2})\Delta t$, $\quad k_3 = f(x_n + \frac{k_2}{2}, t_n + \frac{\Delta t}{2})\Delta t$, $\quad k_4 = f(x_n + k_3, t_n + \Delta t)\Delta t$

The solution in (3.17) is physically interpreted as follow: $k_1 =$ (slope at the beginning of time step). Δt, $k_2 =$ (first approximation to the slope at mid-step).Δt, $k_3 =$ (second approximation to the slope at mid-step).Δt, $k_4 =$ (slope at the end of step).Δt, $\Delta x = \frac{1}{6}(k_1 + 2k_2 + 2k_3 + k_4)$,

Δx is the incremental value of x given by the weighted average estimates based on slopes at the beginning, midpoint, and end of the time step and Δt is the time step.

3.1.2 Implicit integration method

An example of an implicit method is the trapezoidal method [27].

3.1.2.1 Trapezoidal method

This is the simplest implicit integration method. Referring to the differential equation

$$\frac{dx}{dt} = f(x, t)$$ (3.18)

With $x = x_0$ at time, $t = t_0$, the solution for (3.18) at $t = t_1 = t_0 + \Delta t$ is obtained from the integral

$$x_1 = x_0 + \int_{t_0}^{t_1} f(x, \tau)\, d\tau$$ (3.19)

This method uses interpolation techniques as shown in Fig. 3.4 [27] and suggests that functions must pass through the yet unknown point at a time t_1.
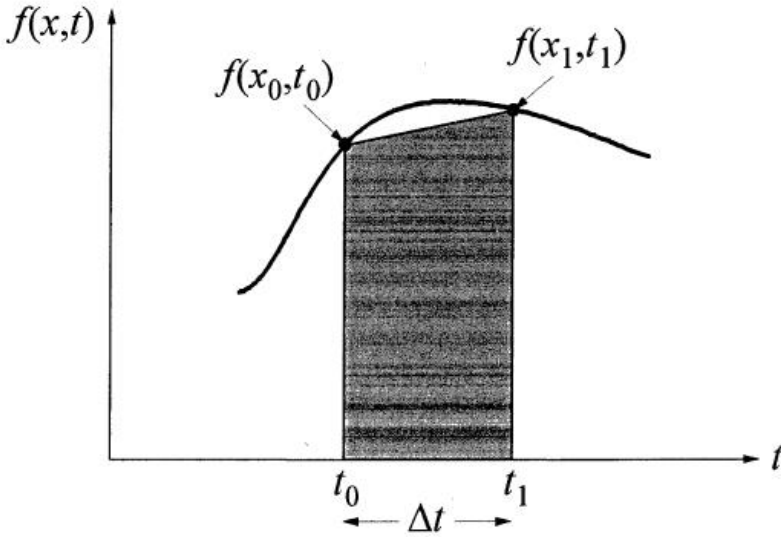
Fig. 3.4: The Trapezoidal method

Equation (3.19) is also expressed as

$$x_1 = x_0 + \frac{\Delta t}{2}[f(x_0, t_0) + f(x_1, t_1)] \tag{3.20}$$

Value of x at $t = t_{n+1}$ is computed as,

$$x_{n+1} = x_n + \frac{\Delta t}{2}[f(x_n, t_n) + f(x_{n+1}, t_{n+1})] \tag{3.21}$$

The trapezoidal rule is a second order method and is numerically stable [27].

3.2 Direct methods

Direct methods are increasingly gaining prominence due to the fact that they do not require the solving of differential equations; instead, they use alternative techniques such as graphical and energy function methods to arrive at a similar solution as numerical methods. Examples of direct methods are the equal area criterion (EAC) and the Lyapunov methods.

3.2.1   The equal area criterion

The Equal Area Criterion (EAC) [27] is a quick way of predicting the stability of a power system without solving the non-linear swing equation. It uses a graphical method to interpret the energy stored in the rotating mass to determine whether the machine preserves its stability following a

disturbance [5]. The method is exclusively applicable to a single-machine system connected to a grid or a two-machine system.

EAC uses the power transfer and swing equations to determine the stability of the system. Rewriting (2.57)

$$\frac{2H}{\omega_0}\frac{d^2\delta}{dt^2} = P_m - P_{max} \sin\delta$$

Where P_m, P_{max}, H, δ, and t denote the mechanical input power in p.u. ignoring frictional losses, the maximum output airgap (electrical) power of the generator in p.u. ignoring damping, the inertia constant (MW. s/MVA), rotor angle in electrical radians, and t time in seconds, respectively.

To demonstrate EAC, we refer to Fig. 3.5 [27], and assuming that the power system is initially stable, and then suddenly mechanical input power changes from an original value P_{m0} to P_{m1} due to a disturbance, the generator will experience a change in rotor angle position. The change will not be instantaneous simply because of inertia possessed by the prime mover and generator. Because of this, the rotor angle changes from δ_0 to δ_1 representing new equilibrium point 'b' where $P_m = P_{m1}$. At this point the mechanical power is greater than the electrical power. This scenario leads to the existence of accelerating power, making the generator rotor accelerate from operating (initial) point 'a' towards point 'b', which is a new equilibrium when traced on the curve $P_e - \delta$ at a rate determined by the swing equation.

The net accelerating power is calculated by the difference between mechanical power, P_{m1}, and electromagnetic power, P_e. The accelerating power at point 'b' is zero, at this point, $\omega_r > \omega_0$. Due to inertia, rotor angle continues to increase and for any value of δ greater than δ_1, $P_e > P_{m1}$ making the rotor begin decelerating reaching a maximum of δ_m, at this point the speed of the rotor ω_r is equal to synchronous speed ω_0, but $P_e > P_{m1}$. Deceleration of the rotor continues while its speed reduces to below ω_0, thus the operating point changes by moving along $P_e - \delta$ curve taking the route 'c'- 'b' - 'a'. It is apparent that rotor the angle is oscillating about δ_1 which is the new equilibrium angle with its amplitude being constant. The plot of δ against time is shown in Fig. 3.5 (b).

The assumptions drawn are: all the resistances, generator damping, and frictional losses are neglected, and the oscillations are only determined by the balance of the two powers.
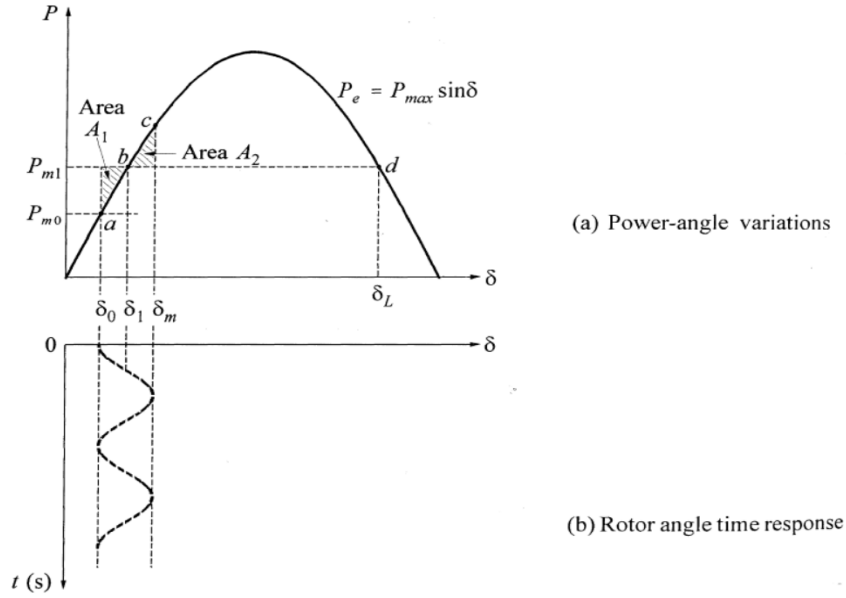
Fig. 3.5: A plot of the power transfer equation and rotor oscillations during a disturbance

EAC presents an alternative method of arriving at the transient stability solution without necessarily solving the swing equation.

Rewriting (2.57)

$$\frac{d^2\delta}{dt^2} = \frac{\omega_0}{2H}(P_m - P_e) \tag{3.22}$$

In (3.22), P_e is a nonlinear function of δ, and therefore, its solution cannot be obtained algebraically. Multiplying both sides of (3.22) by $2\,d\delta/dt$

$$2\frac{d\delta}{dt} \cdot \frac{d^2\delta}{dt^2} = \frac{\omega_0}{H}(P_m - P_e)\frac{d\delta}{dt} \tag{3.23}$$

thus

$$\frac{d}{dt}\left[\frac{d\delta}{dt}\right]^2 = \frac{\omega_0(P_m - P_e)}{H} \cdot \frac{d\delta}{dt} \tag{3.24}$$

Integrating both sides of (3.24) yields:

$$\left[\frac{d\delta}{dt}\right]^2 = \int \frac{\omega_0(P_m - P_e)}{H}d\delta \tag{3.25}$$

The value of speed deviation $d\delta/dt$ is normally zero during normal operations and changes to a definite value when the system is disturbed. To ensure stable operations, the angle deviation δ must be bounded (operate within the limits), and the system should meet a condition where the

33

speed deviation $\frac{d\delta}{dt}$ should be zero after some time following a disturbance. Therefore, (3.25) becomes

$$\int_{\delta_0}^{\delta_m} \int \frac{\omega_0(P_m - P_e)}{H} d\delta = 0 \qquad (3.26)$$

Where δ_0 and δ_m are initial and maximum values for the rotor angles.

Conditions for stability for EAC demands that the integral in equation (3.26) must sum to zero, the area A_1 should be equal to A_2 in Fig.3.3(a), and the Kinetic Energy (KE) gained during acceleration by the rotor should be equal to the energy lost during deceleration.

$$E_1 = \int_{\delta_0}^{\delta_1} (P_m - P_e)\, d\delta = \text{area } A_1 \qquad (3.27)$$

$$E_2 = \int_{\delta_1}^{\delta_m} (P_e - P_m)\, d\delta = area\ A_2 \qquad (3.28)$$

Where E_1 and E_2 are the kinetic energies gained and lost during rotor acceleration and deceleration, respectively. This method is helpful when determining the maximum allowable change in mechanical power P_m before stability is lost. Stability is compromised if the maximum angle $\delta_m > \delta_L$.

3.2.1.1 Determination of the critical clearing angle

A critical clearing angle (CCA) δ_c, is the angle at which the electrical fault must be cleared so that the condition of EAC for stability is achieved [6]. Fig. 3.6 [28] gives a plot of the rotor angle against electrical power. To maintain stability, the two areas, A_1 and A_2 must be equal, otherwise, the stability is lost. Fault clearance beyond the CCA makes the system unstable.

The shaded region A_1 is a function of the time taken for fault clearance. In case of a delay to clear the fault, the critical angle increases, at the same time, the area A_1 increases and the EAC demands that area A_2 also should increase to maintain synchronism at a maximum swing angle δ_{max}. If fault clearance is delayed in such a manner that the rotor angle swings beyond the δ_{max}, the system will be unstable [6]
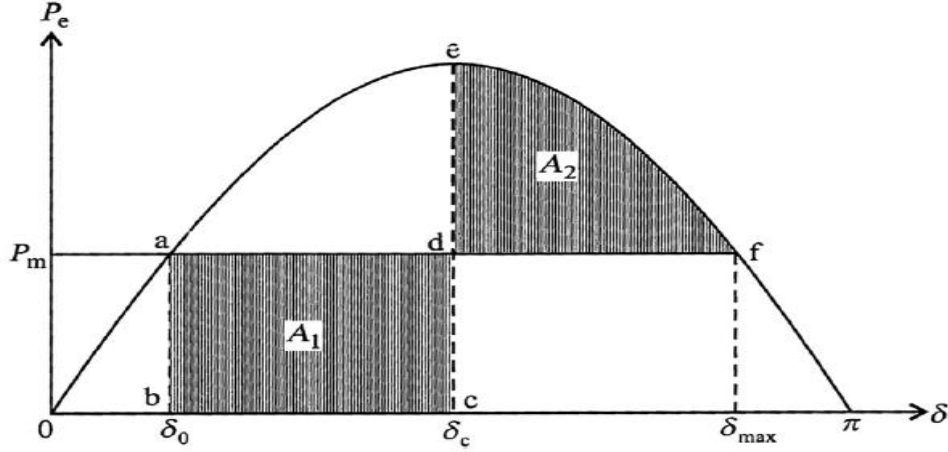
Fig.3.6: The EAC representation of stability

As depicted from Fig. 3.6

$$\delta_{max} = \pi - \delta_0 \tag{3.29}$$

$$P_m = P_{max} \sin \delta_0 \tag{3.30}$$

$$A_1 = \int_{\delta_0}^{\delta_c} (P_m - 0)d\delta = P_m[\delta_c - \delta_0] \tag{3.31}$$

$$A_2 = \int_{\delta_c}^{\delta_{max}} (P_{max} \sin \delta - P_m)d\delta = P_{max}(\cos \delta_c - \cos \delta_{max}) - P_m(\delta_{max} - \delta_c) \tag{3.32}$$

$A_1 = A_2$, yields

$$\cos \delta_c - \cos \delta_m = \frac{P_m}{P_{max}}[\delta_{max} - \delta_0] \tag{3.33}$$

$$\cos \delta_c = \frac{P_m}{P_{max}}[(\pi - \delta_0) - \delta_0] + \cos(\pi - \delta_0)] = \frac{P_m}{P_{max}}[(\pi - 2\delta_0)] - [cos\delta_0] \tag{3.34}$$

Therefore, the critical angle δ_c is given by

$$\delta_c = \cos^{-1}\left[\frac{P_m}{P_{max}}(\pi - 2\delta_0) - (\cos \delta_0)\right] \tag{3.35}$$

3.2.1.2 Determination of critical clearing time

The time corresponding to the critical clearing angle is called the critical clearing time (CCT) t_c [28]. If the fault clearing time is delayed beyond t_c, the two areas, A_1 and A_2 becomes unequal, translating to instability. The CCT t_c is computed from the swing equation as shown by (2.36)

$$\frac{d^2\delta}{dt^2} = \frac{\pi f}{H}(P_m - P_e) \tag{3.36}$$

35

At the time of the fault, $P_e = 0$, thus

$$\frac{d^2\delta}{dt^2} = \frac{\pi f}{H} P_m \qquad (3.37)$$

applying integral on both sides,

$$\int_0^t \frac{d^2\delta}{dt^2} dt = \int_0^t \frac{\pi f}{H} P_m \, dt$$

$$\frac{d\delta}{dt} = \frac{\pi f}{H} P_m t \qquad (3.38)$$

Integrating further gives,

$$\delta = \frac{\pi f}{2H} P_m t^2 + K \qquad (3.39)$$

At t = 0, $\delta = \delta_0$, $K = \delta_0$

Substituting the values in (3.39) and letting $\delta = \delta_c$ gives,

$$\delta_c = \frac{\pi f}{2H} P_m t_c{}^2 + \delta_0 \qquad (3.40)$$

Making t_c the subject of formula gives

$$t_c = \sqrt{\frac{2H(\delta_c - \delta_0)}{P_m \pi f}} \text{ seconds} \qquad (3.41)$$

Factors influencing the CCT are the machine inertia constant, the initial mechanical power, and the load angle. Steam generators have a higher inertia constant than hydro machines, and therefore, the clearing time for steam generators is much higher than for hydro generators.

3.2.2 The Liapunov method

Just like the EAC, the Liapunov's direct method does not require solving the differential equation to arrive at a solution to the transient stability problems; alternatively, it uses the energy function method to obtain solutions to the same problems [29].

It states that for a function

$$\dot{X} = f(X) \qquad (3.42)$$

If there exists a positive definite continuous function *V(X)* whose first partial derivative with respect to the state variable exists and if the total derivative $\dot{V}(X)$ is negative semi definite then the system is said to be stable. Then the function *V(X)* is referred to as Lyapunov energy function.

Fig. 3.7 [29] shows a rolling ball analogy that demonstrates energy balance between kinetic and potential during a power system disturbance.
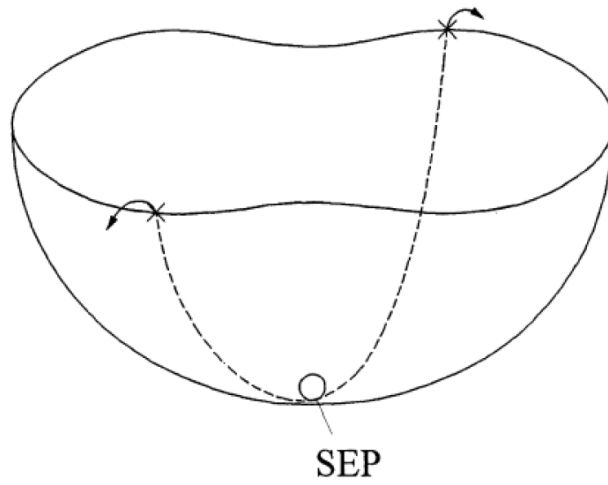
Fig. 3.7: Rolling ball analogy for the Liapunov method

Initially, the ball at the bottom of the bowl is at rest at its stable equilibrium point (SEP). When some kinetic energy (KE) is applied to the ball, it will roll up on the surface inside the bowl, taking a path that depends on the initial direction of the motion.

The ball will stop at a point determined by the amount of KE initially applied. If all the KE is converted to potential energy (PE) prior to reaching the rim, it will roll back and finally settle down at the SEP. However, if the KE applied is huge enough to make the ball go over the rim, then the ball enters the instability region and fails to return to the SEP. The surface inside the ball represents the PE surface, and the rim represents the potential energy boundary surface (PEBS).
The two quantities that determine whether the ball enters into instability or not are the initial applied KE and the rim's height.

The same concept is used in power systems to determine stability. For a given system fault, the KE must be converted into PE before attaining a critical point; otherwise, the system becomes unstable. This technique is referred to as the transient energy function (TEF). A function can be derived to define the transient energy of the system and critical energy needed to cause system instability [29].
Referring to the swing equation in (2.57), for the synchronous generator connected to a power system

37

$$\frac{2H}{\omega_0}\frac{d^2\delta}{dt^2} = P_m - P_{max}\,\sin\delta$$

By letting the potential energy function be a function of the rotor angle δ

$$V_{PE}(\delta) = -P_m\delta - P_{max}\,\cos\delta \tag{3.43}$$

Thus,

$$\frac{2H}{\omega_0}\frac{d^2\delta}{dt^2} = P_m - P_{max}\,\sin\delta = -\frac{dV_{PE}(\delta)}{d\delta} \tag{3.44}$$

Multiplying both sides (3.44) by $\frac{d\delta}{dt}$, rearranging and taking and taking $M = \frac{2H}{\omega_0}$ yields

$$\frac{d}{dt}\left(\frac{1}{2}M\left(\frac{d\delta}{dt}\right)^2\right) + \frac{dV_{PE}(\delta)}{dt} = 0 \tag{3.45}$$

Given that δ_0 is the initial rotor angle, then

$$V_{PE}(\delta, \delta_0) = -P_m(\delta - \delta_0) - P_{max}(\cos\delta - \cos\delta_0) \tag{3.46}$$

Defining the total energy of the system as an energy function

$$V(\delta, \omega') = \frac{1}{2}M(\omega')^2 - P_m(\delta - \delta_0) - P_{max}(\cos\delta - \cos\delta_0) \tag{3.47}$$

Fig. 3.8 [29] shows the power and energy conversion curves for the Lyapunov method.
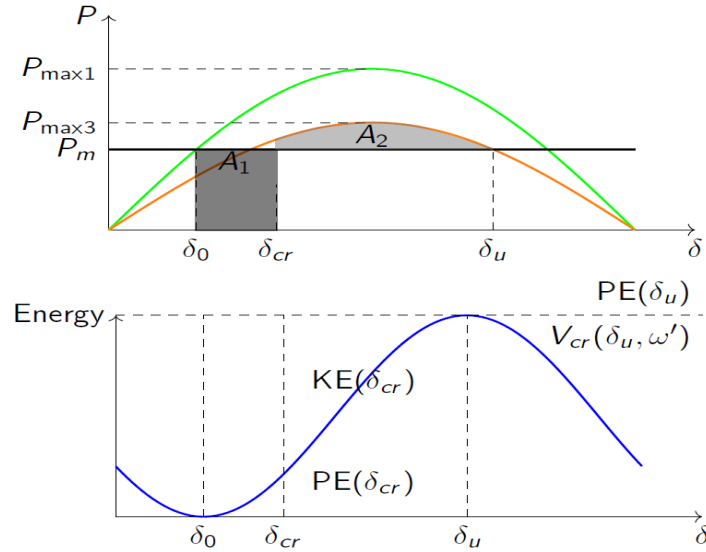

Fig. 3.8: Power angle and energy conversion curves for Lyapunov method

For stability to be guaranteed,

$$A_1 = A_2$$

$$PE(\delta_{cr}) + KE(\delta_{cr}) = PE(\delta_u)$$

At the rotor angle δ_u, the transient energy is

$$V_{cr}(\delta_u, \omega') = \frac{1}{2}M(\omega')^2 - P_m(\delta_u - \delta_0) - P_{max}(\cos\delta_u - \cos\delta_0) \tag{3.48}$$

The energy $V_{cr}(\delta_u, \omega')$ is the maximum energy the system can attain without losing stability. If it exceeds this value, then the system becomes unstable. Therefore, assessment of system stability is done by calculating the transient energy at the CCA and comparing it with $V_{cr}(\delta_u, \omega')$, which should be lower.

At the CCA, the transient energy is given by (3.49)

$$V_{cl}(\delta_{cr}, \omega') = \frac{1}{2}M(\omega')^2 - P_m(\delta_{cr} - \delta_0) - P_{max}(\cos\delta_{cr} - \cos\delta_0) \tag{3.49}$$

In summary,

    (i) If $V_{cl}(\delta_{cr}, \omega') \leq V_{cr}(\delta_u, \omega')$, the system is stable.

    (ii) If $V_{cl}(\delta_{cr}, \omega') > V_{cr}(\delta_u, \omega')$, the system is unstable.

3.3 Why equal area criterion is preferred

As stated in Section 3.2.1, the equal area criterion (EAC) is applied in a situation where the analysis is based on a single-machine or two-machine system connected to an infinite bus. The method provides a physical understanding of the machine's dynamic behavior during disturbances. Also, this method, when compared to Lyapunov, which involves complex integration formulas, is convenient because it uses simple algebraic equations to arrive at a transient stability solution. Additionally, it does not require the solving of a non-linear swing equation. EAC is very useful when determining the maximum power that can be added to any power system without compromising its stability [5]. Generally, the method provides a suitable platform for designing the optimal number of transmission power lines, taking into consideration various types of faults and fault locations. These features make EAC a suitable method for this study.

3.4 Conceptual framework

Fig. 3.9 gives the conceptual framework of the thesis. A conceptual framework provides guidelines for the mapping of the interrelated variables and bringing them together to achieve the thesis goals. In the structure, the main research subject is broken down into sub-systems. The rotor angle transient analysis is broken down to show the type of machine, the machine control method, and

the machine operations in terms of the loading. Then, the three objects are included in the model, which is simulated and analyzed to determine the transient stability.
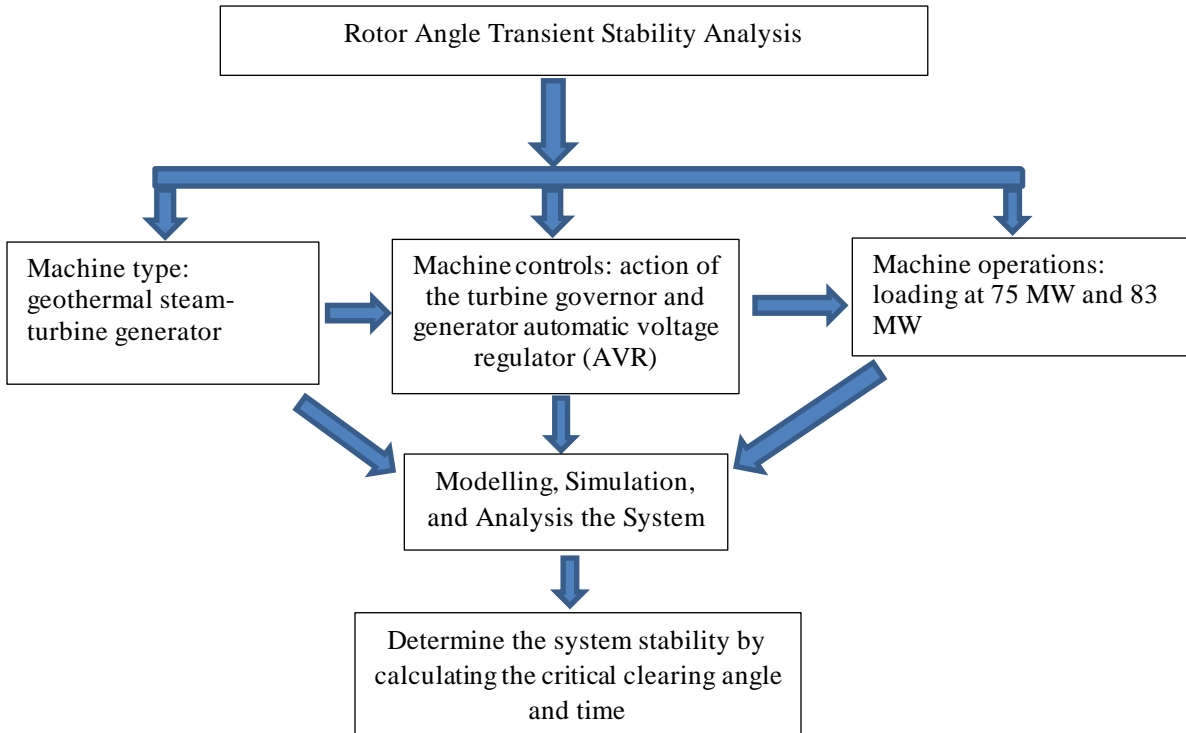

Fig. 3.9: Conceptual framework

3.5 Chapter conclusion

This chapter outlines the methodology employed to arrive at the solution to the transient stability problem. The EAC Commonly available methods have been described, including numerical and direct methods. Each method has been described in detail, indicating its strengths and shortcomings.

CHAPTER 4: RESULTS AND ANALYSIS

This chapter presents the thesis results and analysis. The collected system data is entered into the ETAP model, which is then simulated to generate some results that are analyzed using the appropriate methods to determine the transient stability of the system.

4.1 Analysis of the generator under steady state operation

In this section, three different scenarios are analyzed, involving the operation of the machine at power factors (p.f.) of 0.85 lagging, unity, and 0.95 leading. From the analysis, the rotor angle values for different scenarios will be noted.

4.1.1   Case1: Measured values

Table 4.1 illustrates values obtained from the online measurement of the generator at Olkaria IV operating at its rated capacity and delivering power to the grid.

Table 4.1: Machine parameter values obtained from measurement

NO.	Parameter	Name	Value
1	P_e	Electrical Active Power	74.4 MW
2	E_t	Terminal Voltage	11.31 kV
3	I	Armature Current	3.76 kA
4	p.f.	Power Factor	0.99
5	Q	Reactive Power	0.5 MVAr
6	S	Apparent Power	88.55MVA
7	RPM	Generator Speed	3000 RPM

Data from manufacturer: H = 3.385 (inertia constant), $X_g = 189\%$ (generator synchronous reactance). Revisiting (2.55) of a synchronous generator and rewriting

$$P_e = \frac{E_f E_t}{X_g} \sin\delta = P_{max} \sin\delta \tag{4.1}$$

Where X_g denotes the generator synchronous reactance (steady state), E_f denotes the generator voltage behind transient reactance proportional to field flux, E_t denotes the generator terminal voltage, and δ denotes the rotor angle. During steady-state operation, generator rotor mechanical power (P_m) is equal to electrical power or air gap power (P_e). Speed is maintained at a constant and the rotor angle δ does not change. From the measured values and data provided by the manufacturer, the rotor angle δ can be calculated using (4.1). Given that $P_e = P_m$ during steady

state operation, the rotor angle is calculated as follows:

Computing the $E_f \angle \delta$ for the synchronous generator, where E_f is expressed in kV.

$$E_f = E_t \angle \phi + jIX_g \tag{4.2}$$

$$\phi = \cos^{-1} pf = \cos^{-1} 0.99 = 8.11°$$

$$E_f = 11.31 \angle \phi + j3.76X_g$$

$$X_{g,actual} = X_{g,pu} \times X_{g,base}$$

$$X_{g,base} = \frac{(\text{Base kV})^2}{\text{Base MVA}} = \frac{11^2}{88.55} = 1.37\Omega$$

$E_f = 11.31 \angle 8.11° + (3.76 \times j1.37) = 11.20 + j6.74 = 13.07 \angle 31.07°$ kV

Substituting values in equation (4.1) and using E_f to compute δ

$$74.44 = \frac{13.07 \times 11.31 \sin \delta}{1.37} = 107.90 \sin \delta \ ; \sin \delta = 0.6899; \ \delta = 43.62°$$

4.1.2   Case 2: 75MW at 0.85 Lagging p.f, Unity and 0.95 Leading p.f.

The assumptions made during the calculations are that the generator terminal voltage is maintained constant at 11 kV, the airgap flux is maintained constant, and the excitation current is maintained constant.

4.1.2.1 p.f. = 0.85 lagging

Armature current I, flowing through the circuit is

$$I = \frac{\text{MVA}}{\sqrt{3} \times V_{LL}} = \frac{88.55}{\sqrt{3} \times 11} = 4.65\text{kA}$$

With p.f. of 0.85, $\emptyset = 31.79°$, V_{LL} is the generator terminal voltage, line to line.

Substituting value in (4.2), E_f is arrived at

$E_f = 11.00 \angle 31.79° + (4.65 \times j1.37) = (9.35 + j5.79) + j6.37 = 15.34 \angle 52.45°$ kV

Using E_f to compute δ

$$75 = \frac{15.34 \times 11.00 \sin \delta}{1.37} = 123.17 \sin \delta; \ \sin \delta = 0.6089; \ \delta = 37.51°$$

4.1.2.2 p.f. = 1 (unity)

With p.f. of unity, $\emptyset = 0°$,

$E_f = 11.00\angle 0° + 4.65 \times j1.37 = 11.00 + j6.37 = 12.71\angle 30.07°$

using E_f to compute δ

$75 = \frac{12.71 \times 11.00 \sin \delta}{1.37} = 102.05 \sin \delta; \sin \delta = 0.7349; \delta = 47.30°$

4.1.2.3 p.f. = 0.95 leading

With p.f. of 0.95 leading, $\emptyset = -18.19°$,

$E_f = 11.00\angle - 18.19° + (4.65 \times j1.37) = (10.45 - j3.43) + j6.37 = 10.85\angle 15.69° \text{ kV}$

using E_f to compute δ

$75 = \frac{10.85 \times 11.00 \sin \delta}{1.37} = 87.12 \sin \delta; \sin \delta = 0.8609; \ \delta = 59.42°$

4.1.3   Case 3: 83 MW at 0.95 lagging p.f., unity and 0.95 leading p.f.

The corresponding values of the rotor angle are calculated from the three different cases of p.f. operations.

4.1.3.1 p.f. = 0.95 lagging

With p.f. of 0.95, $\emptyset = 18.19°$,

$E_f = 11.00\angle 18.19° + (4.65 \times j1.37) = (10.45 + j3.43) + j6.37 = 14.33\angle 43.17° \text{ kV}$

Using E_f to compute δ

$83 = \frac{14.33 \times 11.00 \sin \delta}{1.37} = 115.06 \sin \delta; \sin \delta = 0.7214; \delta = 46.17°$

4.1.3.2 p.f. = 1 (unity)

With p.f. of unity, $\emptyset = 0°$,

$E_f = 11.00\angle 0° + 4.65 \times j1.37 = 11.00 + j6.37 = 12.71\angle 30.07° \text{ kV}$

Using E_f to compute δ

$83 = \frac{12.71 \times 11.00 \sin \delta}{1.37} = 102.05 \sin \delta; \sin \delta = 0.8133; \delta = 54.42°$

4.1.3.3 p.f. = 0.95 leading

With p.f. of 0.95 leading, $\emptyset = -18.19°$,

$E_f = 11.00\angle - 18.19 + 4.65 \times j1.37 = (10.45 - j3.43) + j6.37 = 10.85\angle 15.69° \text{ kV}$

Using E_f to compute δ

$83 = \dfrac{10.85 \times 11.00 \sin \delta}{1.37} = 87.12 \sin\delta; \sin\delta = 0.9527; \delta = 72.32°$

The summary of the rotor angle computation at different power factors are presented in Table 4.2. The effect of excitation or power factor on transient stability can be analyzed using phasor diagrams shown in Figs. 4.1–4.2. The figures show the variation in rotor angle with different operating values of machine power factor. Operating at a power factor of 0.85 lagging, unity, and 0.95 leading corresponds to the following rotor angles: 37.5 degrees, 47.3 degrees, and 59.4 degrees, respectively. It is therefore concluded that a machine running with reduced excitation or a higher power factor is more susceptible to instability. The parameters, ωs and ωr are synchronous speed and rotor speed, respectively, and δ is the rotor angle.

Table 4.2: Calculated values of machine parameters

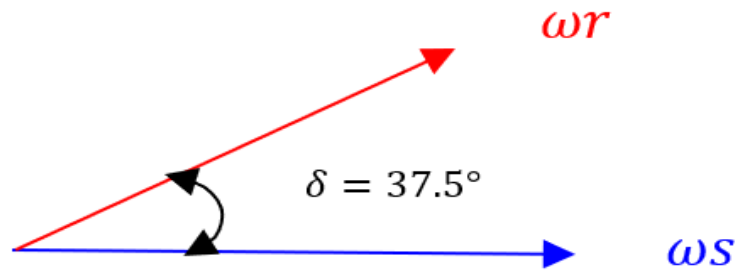| NO	P_m(MW)	p.f.	P_{max} (MW)	$\sin\delta$	δ (degrees)
1	74.44 (ONLINE)	0.99 (lagging)	107.90	0.6899	43.6
2	75	0.85 (lagging)	123.17	0.6089	37.5
3	75	1 (unity)	102.50	0.7349	47.3
4	75	0.95 (leading)	87.12	0.8609	59.4
5	83	0.95 (lagging)	115.06	0.7212	46.1
6	83	1(unity)	102.05	0.8133	54.4
7	83	0.95 (leading)	87.12	0.9527	72.3

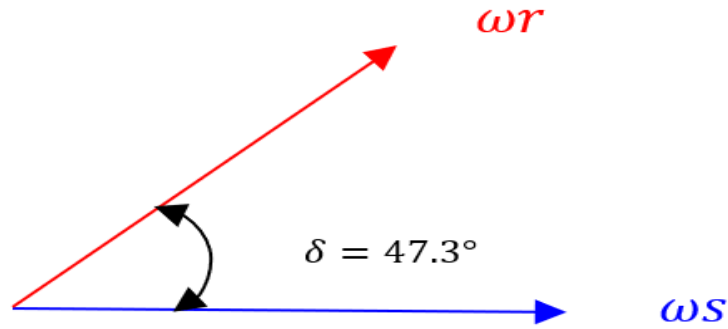*Fig. 4.1: A Phasor diagram of a machine at 75 MW, 0.85 lagging p.f.*

Fig. 4.2: A Phasor diagram of a machine at 75 MW, unity p.f.
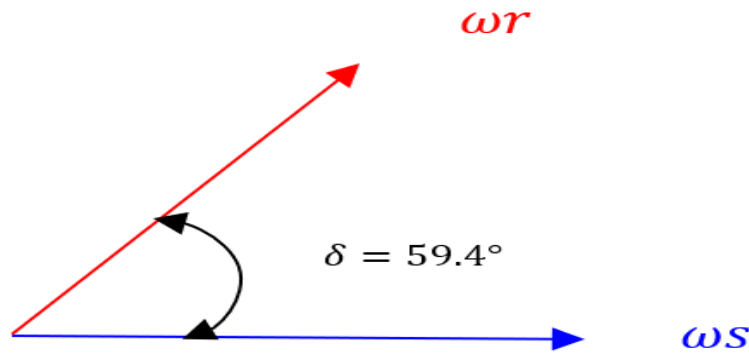
Fig. 4.3: A Phasor diagram of a machine at 75 MW, 0.95 leading p.f.

4.2 Modeling of the swing equation

Fig. 4.4 shows a block diagram of a swing equation (2.57). The diagram is composed of the summer, summing up P_e and P_m, the gain amplifier, and the integrator output. The output of the system is the rotor angle δ. The system is modeled as shown Fig. 4.5 using a Simulink tool in MATLAB and simulated. From the simulation, the rotor angles against time were plotted for different offsets in the electrical and mechanical powers. The model parameters were obtained from the Olkaria IV machine data, as shown in Appendix B. The model neglected the damping factor K_D because the time constant of the damper circuit is greater than the transient stability period.
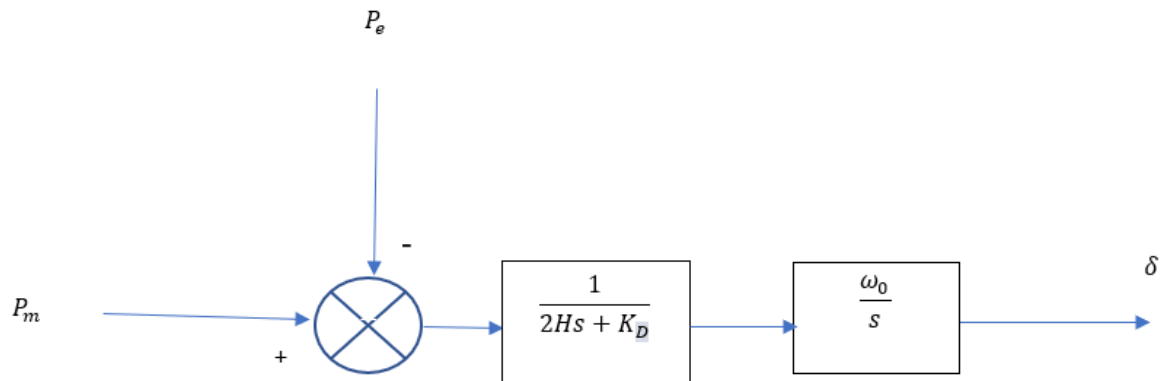
Fig. 4.4: A block diagram of the swing equation

$H = 3.385, \ 2H = 2 \times 3.385 = 6.77, \ K_D = 0 \ \text{and} \ \omega_0 = 1$
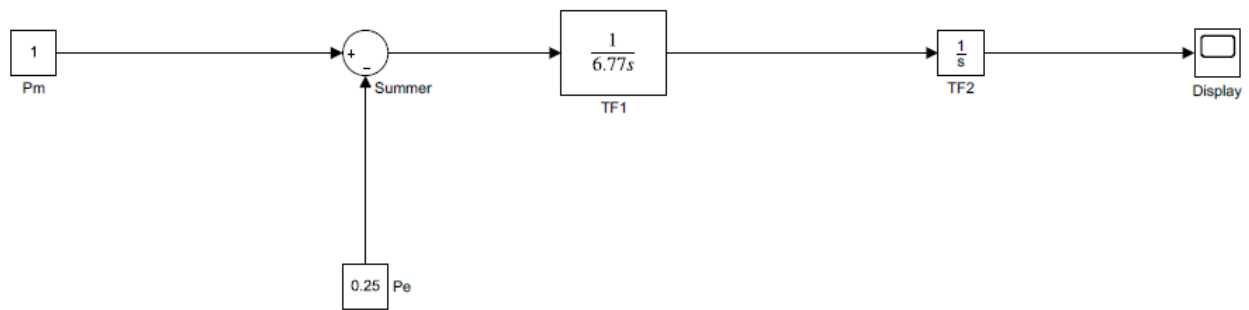
Fig. 4.5: A Simulink model of the swing equation

Fig. 4.6 shows a plot of generator rotor angle (p.u) versus time (sec). The change in rotor-angle position with time indicates acceleration due to an imbalance between mechanical and electrical powers. With 0% deviation, the rotor angle position does not change.
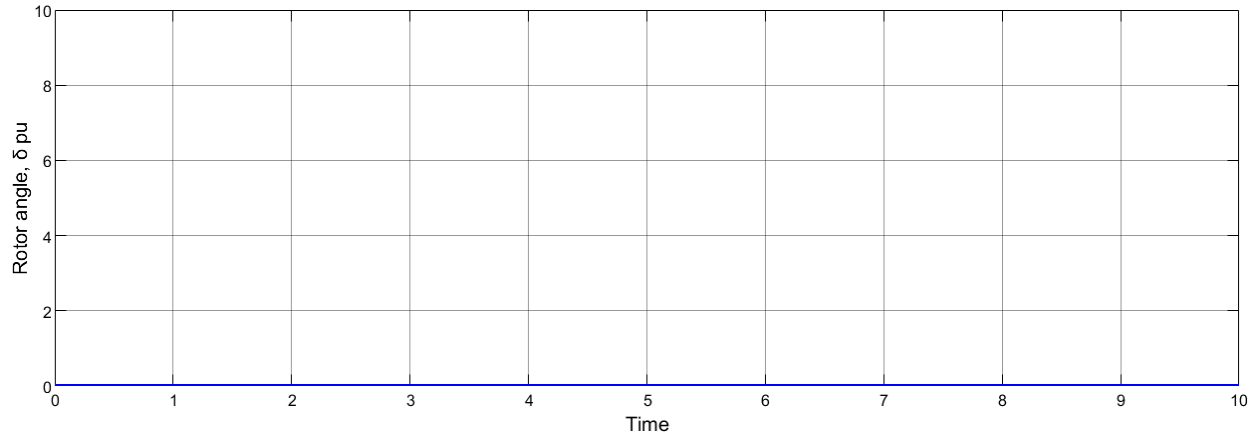
Fig. 4.6: A plot of a rotor angle (δ) versus time(sec) for 0% power offset

For the 50% power deviation between electrical and mechanical, the plot of generator rotor angle (δ) versus time (sec) for is shown by Fig. 4.7. The rate of change translates to 3.7 units of rotor angles in 10 seconds.
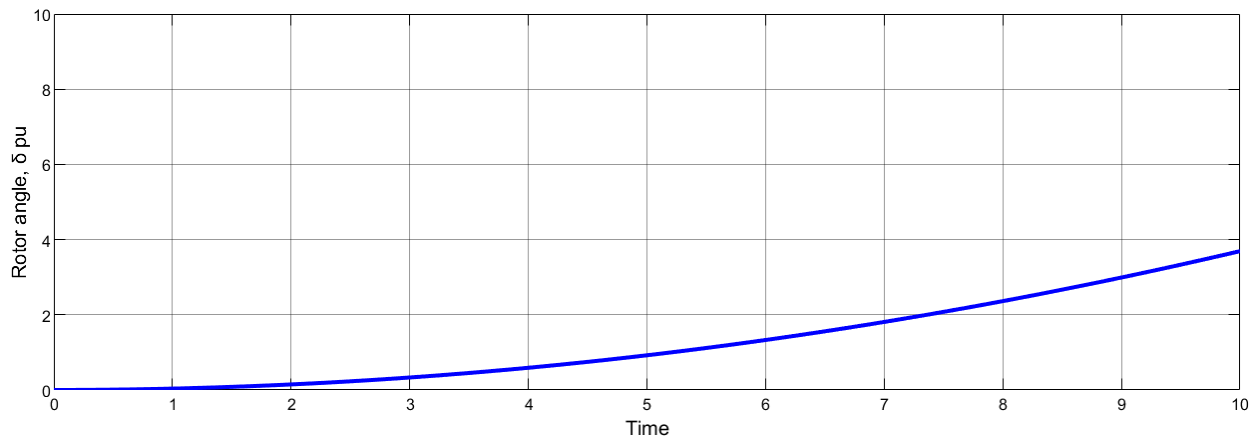
Fig. 4.7: A plot of a rotor angle (δ) versus time(sec) for 50% power offset

As the deviation increases to 75%, the rate of change of the rotor angle increases as well, as shown in Fig. 4.8. At this point, the rotor angle increases by 5.4 units in 10 seconds.
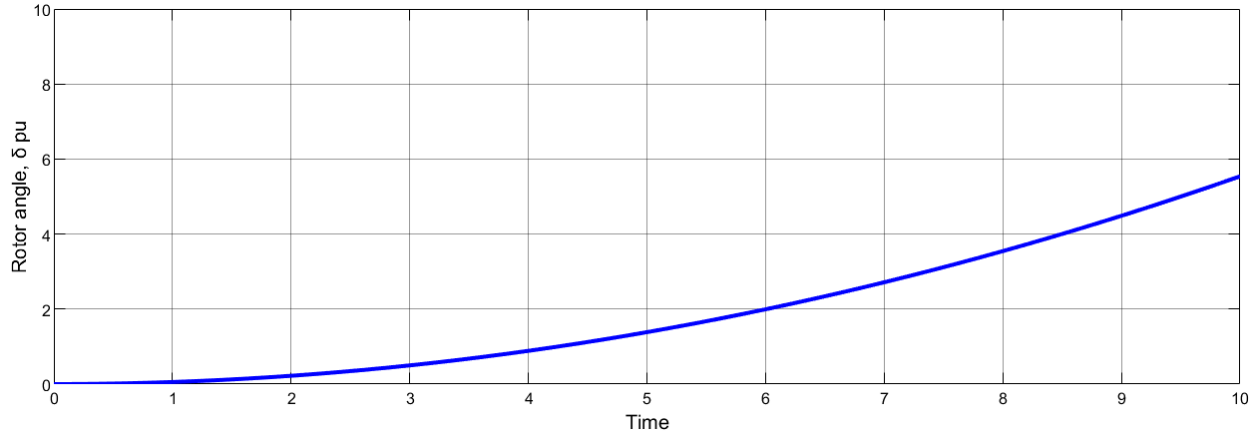
Fig. 4.8: A plot of a rotor angle (δ) versus time(sec) for 75% power offset

When the power difference between mechanical and electrical is 100%, the rotor angle rate of change increases to 7.4 units in 10 seconds. See Fig. 4.9.
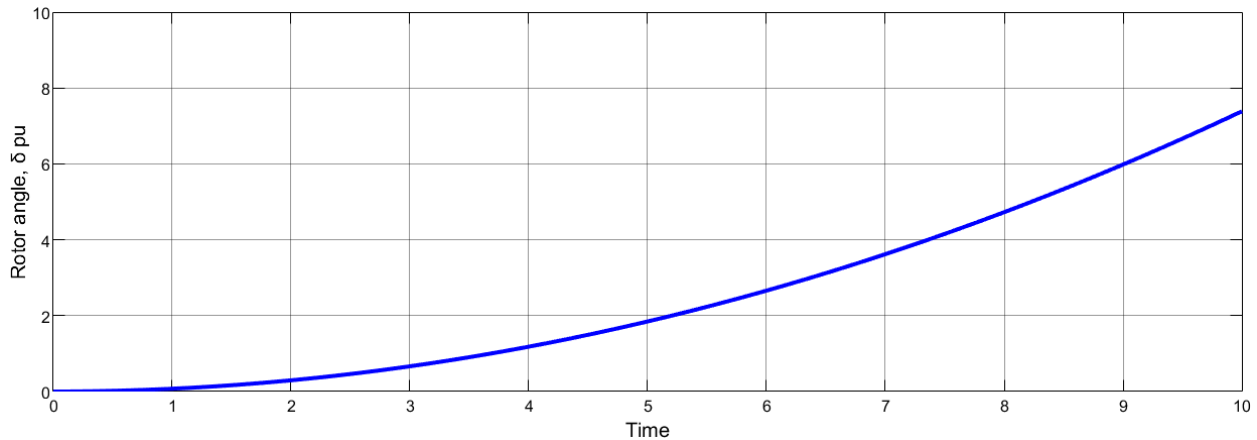
Fig. 4.9: A plot of a rotor angle (δ) versus time(sec) for 100% power offset

Practically, machines respond to system disturbances and act appropriately to minimize the effects of deviations using the generator automatic voltage regulator (AVR) and turbine governor, unless the disturbance is severe. The AVR controls voltage and VARS, while the turbine governor controls speed and active power.

4.3 System modelling and power flow analysis

Fig. 4.10 represents an electrical model of the Olkaria IV generator connected to the grid through a step-up transformer. The model was developed using the ETAP software, and it is made up of a

48

synchronous generator, a power transformer, buses, transmission lines, and the system load. The model was subjected to power flow and transient stability analysis to generate some values.
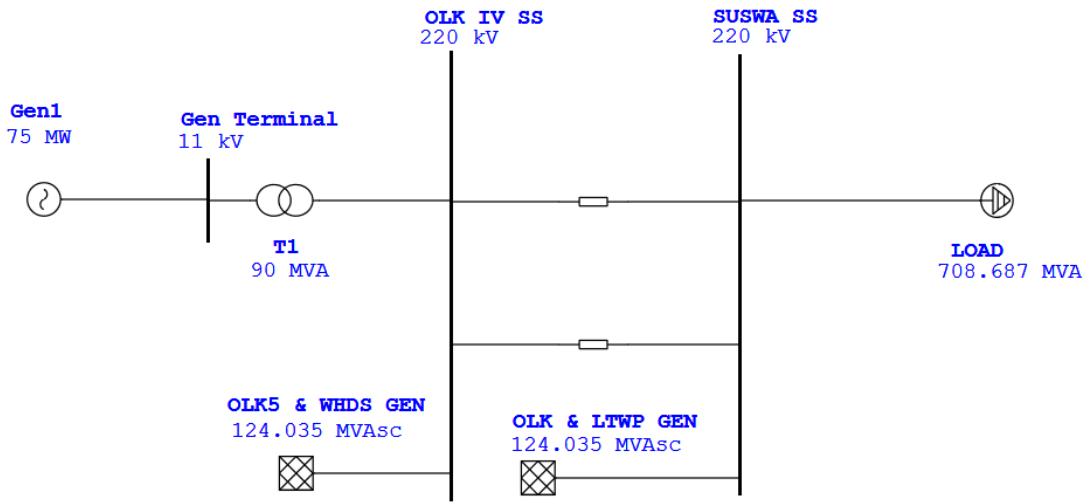
Fig. 4.10: Electrical model of Olkaria IV generator connected to the power system

The 75 MW machine operating at a lagging power factor of 0.85 at steady state is represented in Fig. 4.11. Power system parameters appearing in the figure are generated by running the power flow function in the ETAP program.
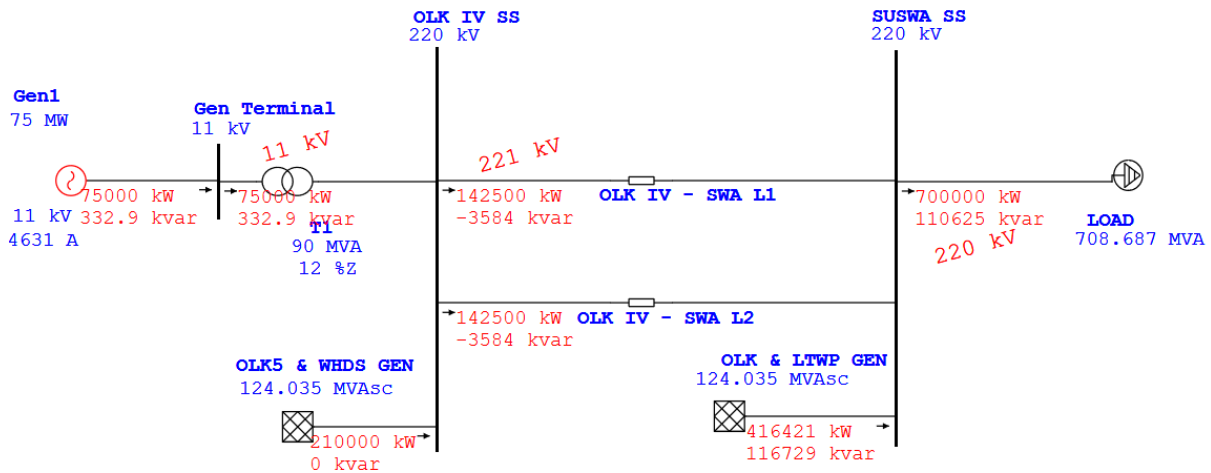
Fig. 4.11: Power-flow simulation for a machine at 75MW, 0.85 lagging p.f. at steady-state

The 83 MW machine operating at a lagging power factor of 0.95 at steady state is represented in Fig. 4.12. The power system parameters appearing in the figure are generated by running the power

flow function in the ETAP program. Other power sources included in the model are Wellheads (WHDS) power generation, Olkaria 5, and Lake Turkana wind power (LTWP).
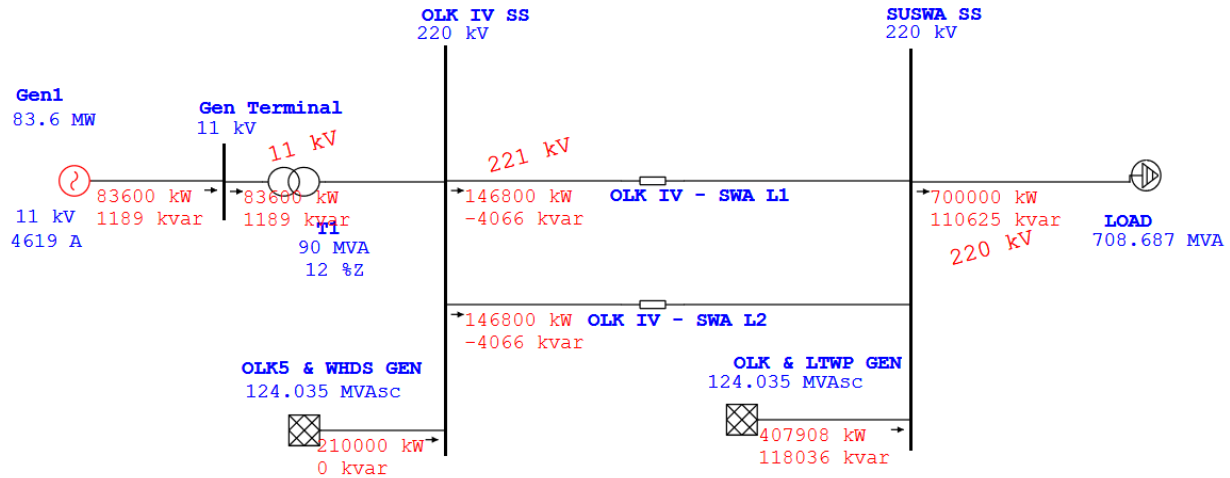
Fig. 4.12: Power-flow simulation for a machine at 83MW, 0.95 lagging p.f. at steady-state

4.4 Transient stability analysis

Transient stability analysis is a time-domain tool used to show the time response of the power system parameters. The areas of interest in transient stability studies include the behavior of the system during pre-fault, fault, and post-fault. In this case, the transient analysis was carried out by considering a duration of 10 seconds, as recommended by [8], and the fault clearing time of 0.1 seconds. The fault clearing time of 0.1 seconds was chosen after factoring in the breaker opening time, which is about 2 cycles (40 ms) [30]. The simulation time step size was selected to be 0.001 for better accuracy [8].

4.4.1   Generator operation at 75 MW, 0.85 lagging p.f.

Transient stability analysis for 75 MW machine indicate the initial rotor angle value of 9.88°, as shown in Fig. 4.13.
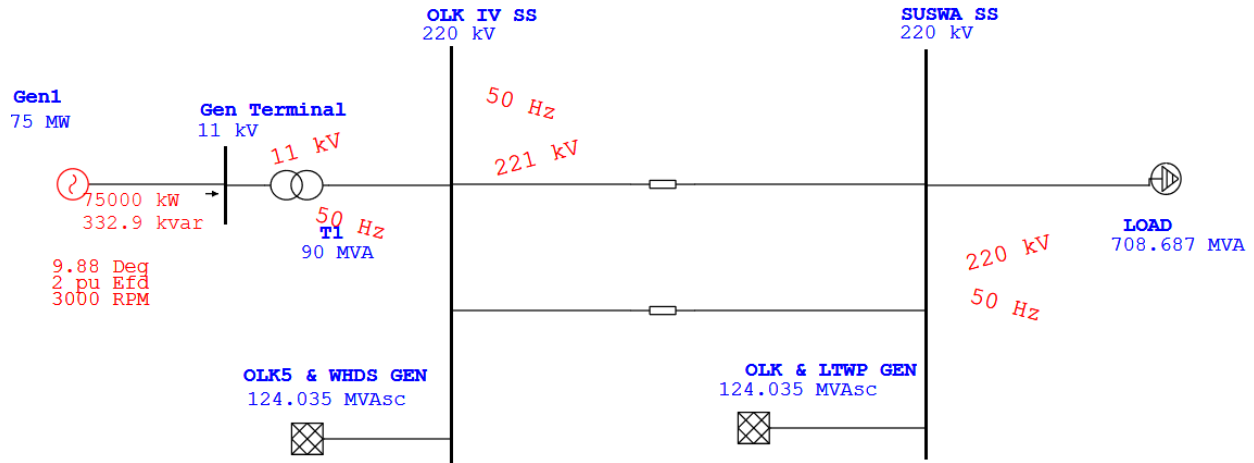
Fig. 4.13: Pre-fault state for a machine at 75 MW

Fig. 4.14 illustrates a faulted state of the power system; the fault lasted for one second. The effects of the fault have been felt by the system, causing the generator's electrical power output to fall to zero and bus voltages to get depressed. Voltages closer to the fault fall to zero, while locations far from the fault are less affected. This is due to the impedance of the electrical equipment. It was also noted that the system frequency remained constant.
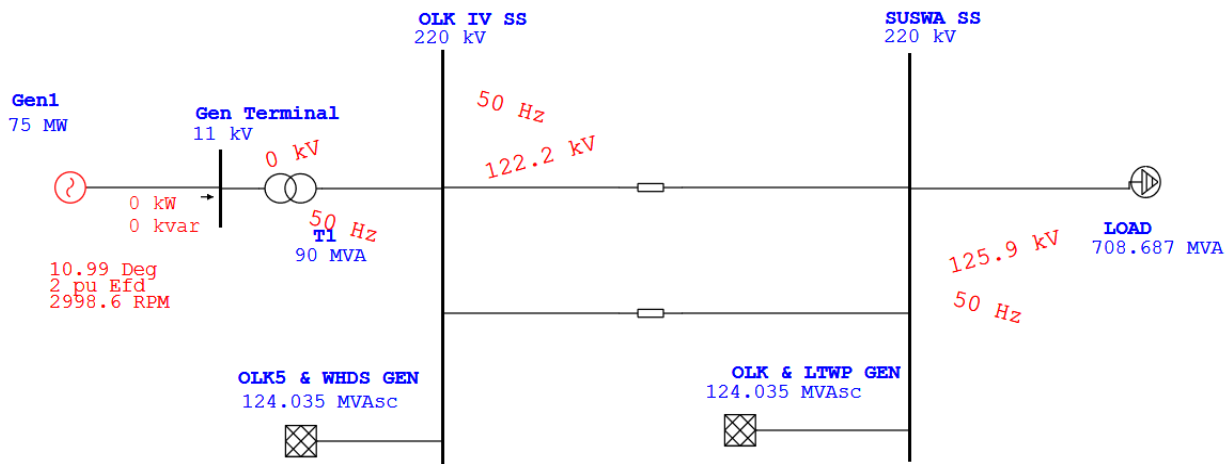
Fig. 4.14: Fault state for a machine at 75 MW

4.4.2   Generator operation at 83 MW, 0.95 lagging p.f.

Transient stability analysis for 83 MW machine indicate the initial rotor angle value of 13.58°, as shown in Fig. 4.15
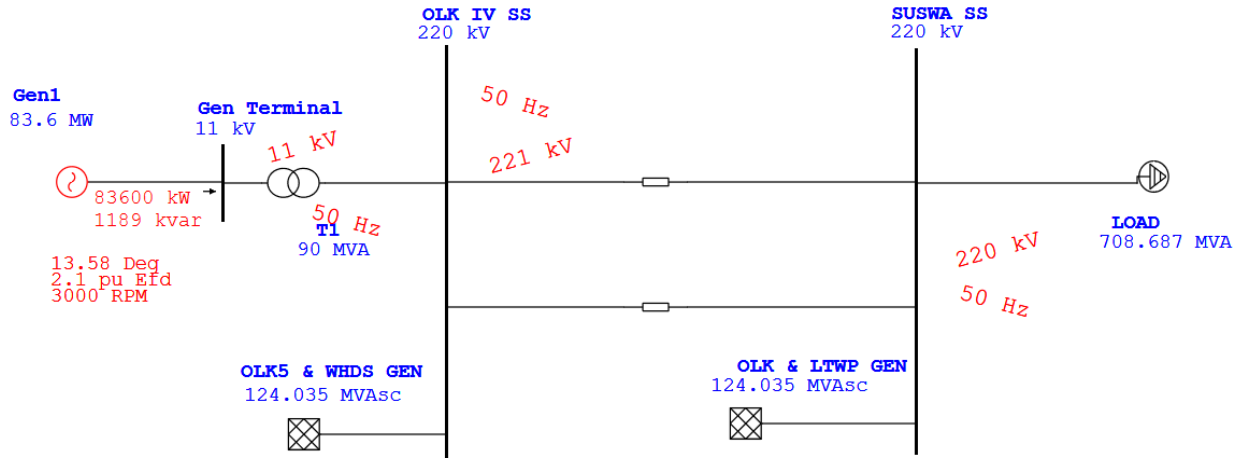
Fig. 4.15: Pre-fault state for a machine at 83MW

Fig. 4.16 illustrates the faulted state of the power system; the fault lasted for one second. The effects of the fault on the system for the 83 MW machine were similar to those for the 75 MW machine.
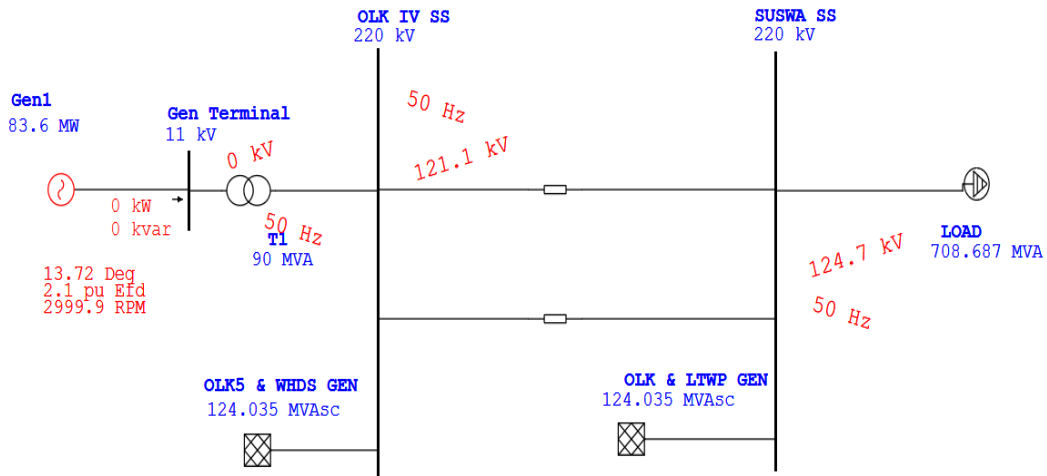
Fig. 4.16: Fault state for a machine at 83MW

4.4.3 Plots of the critical power system parameters

Figs. 4.17 and 4.18 show plots of rotor angle against time for the 75 MW and 83 MW machines, respectively, during a fault. The plots exhibit oscillations of the rotor angle, whose amplitude decays with time. The 85 MW machine experiences greater rotor angle swings with a maximum amplitude of 44° when compared to the 75 MW machine, with a maximum amplitude of 38°.
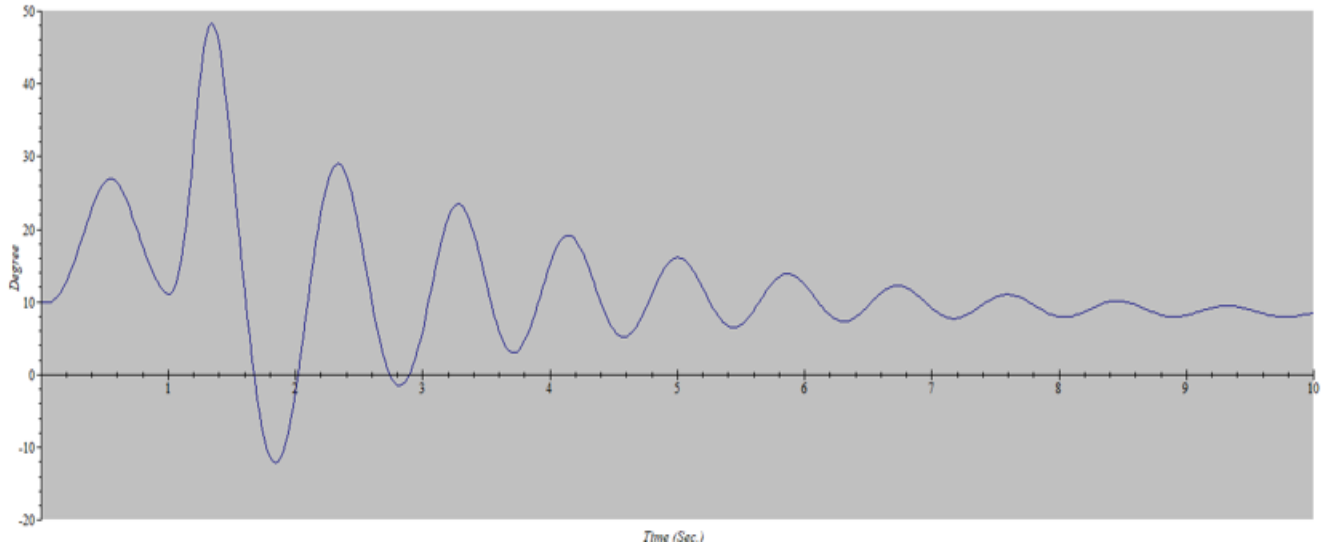
Fig. 4.17: A plot of a rotor angle versus time for a 75MW machine
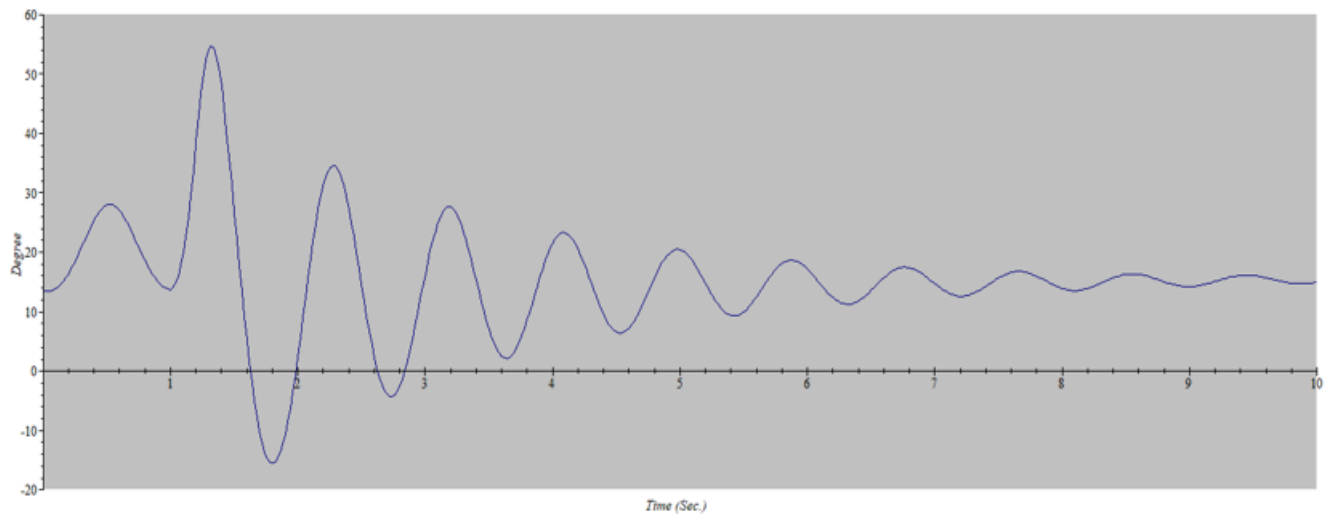
Fig. 4.18: A plot of a rotor angle versus time for a 83 MW machine

For electrical power, when plotted against time for the 75 MW and 83 MW machines, the latter experienced a maximum swing of about 300% of its rated power as compared to 240% for the 75 MW machine, as shown in Figs. 4.19 and 4.20. The graphs for both cases contain notches resulting from harmonics generated as a result of the magnetic core saturation of the generator.
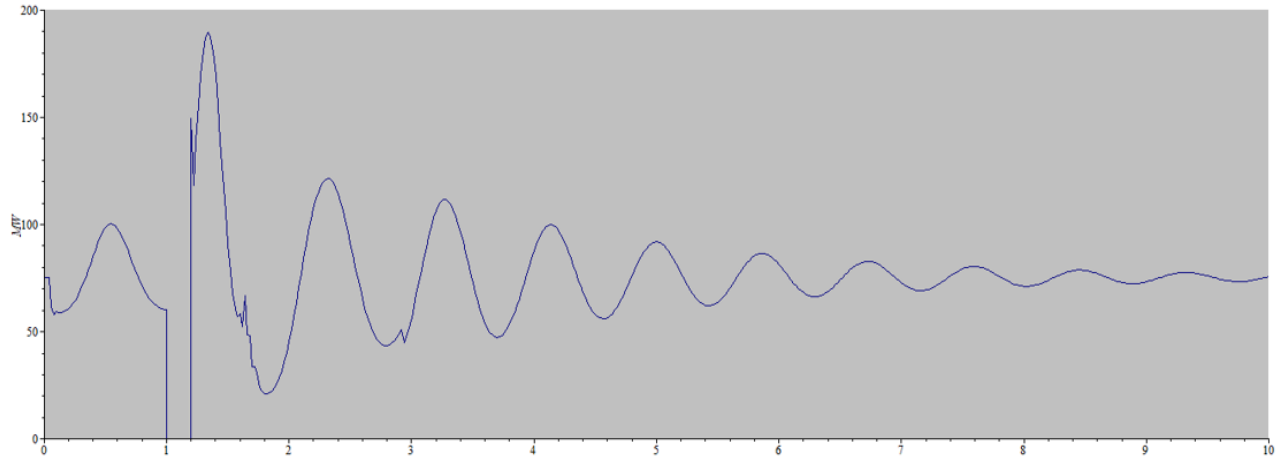
Fig. 4.19: A plot of electrical power versus time for a 75 MW machine
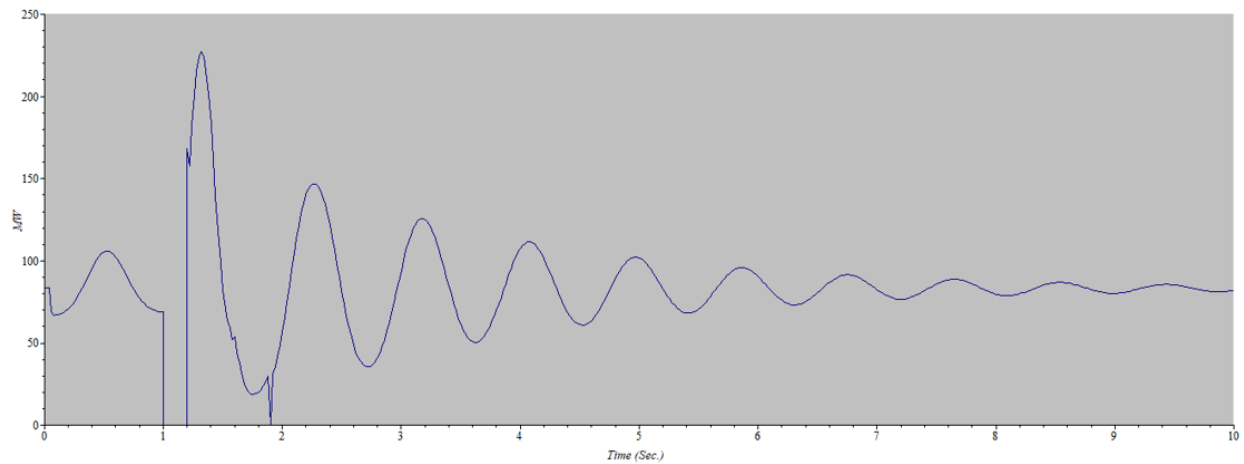
Fig. 4.20: A plot of electrical power versus time for a 83 MW machine

The mechanical time plots for mechanical power for 75 MW and 83 MW machines are shown in Figs. 4.21 and 4.22, respectively. The graphs indicate constant mechanical power throughout the fault duration. This is attributed to the fact that turbine governor action is not considered during the transient stability studies. This is because it has a time constant that is much higher than the 10 seconds recommended for transient stability [17].
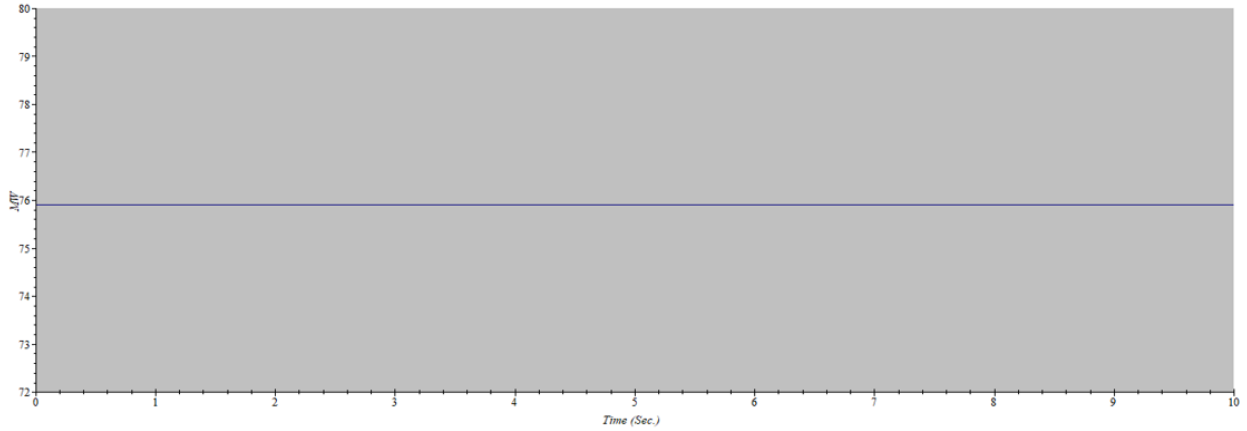
Fig. 4.21: A plot of mechanical power versus time for a 75 MW machine
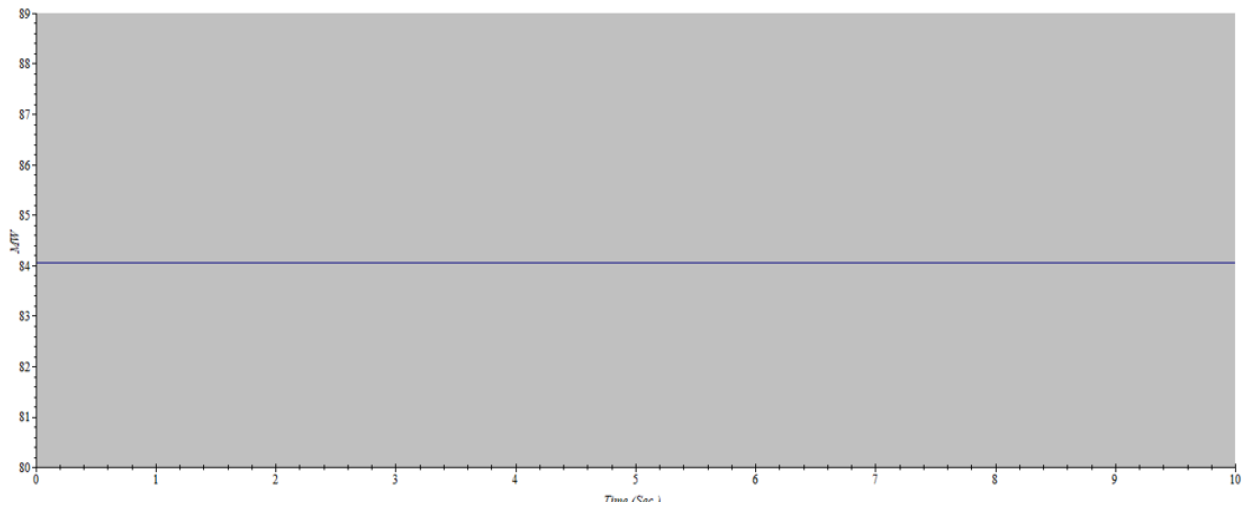
Fig. 4.22: A plot of mechanical power versus time for a 83 MW machine

For a machine operating in synchronism, its speed translates to the frequency of the system. Therefore, monitoring this parameter is crucial because any deviation is detrimental. High speeds may lead to bearing failure and stresses in the turbine blades, while low speeds affect the machine's cooling and may cause resonance. Figs. 4.23 and 4.24 show variation of the generator speed with time for both machine ratings. The generator speed in RPM and the magnetic poles together determine the frequency of the electrical signal. During transient conditions, the maximum speed attained by the 83 MW machine is 3036 rpm, as compared to the 75 MW machine, which attained 3031 rpm.
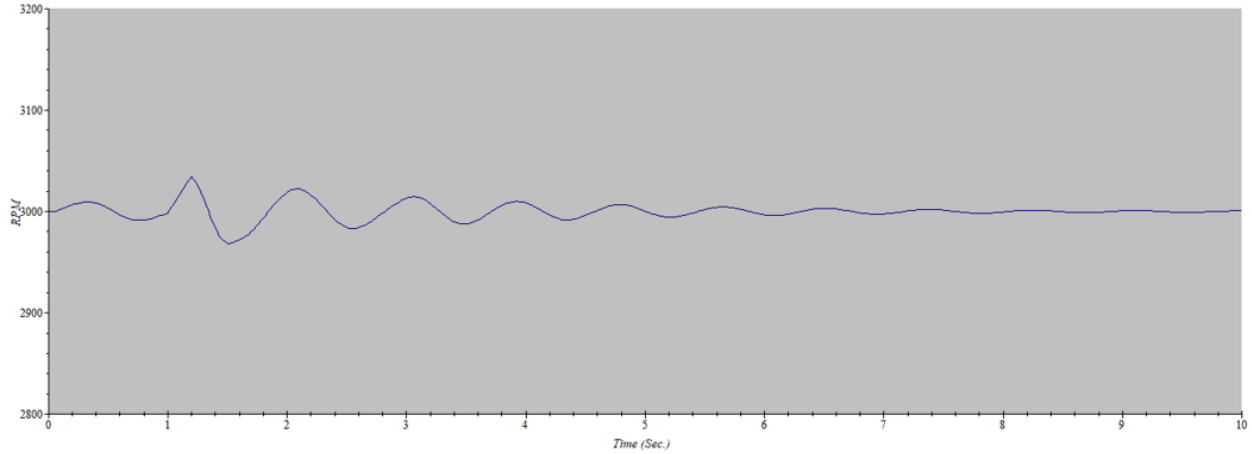
Fig. 4.23: A plot of generator speed versus time for a 75 MW machine
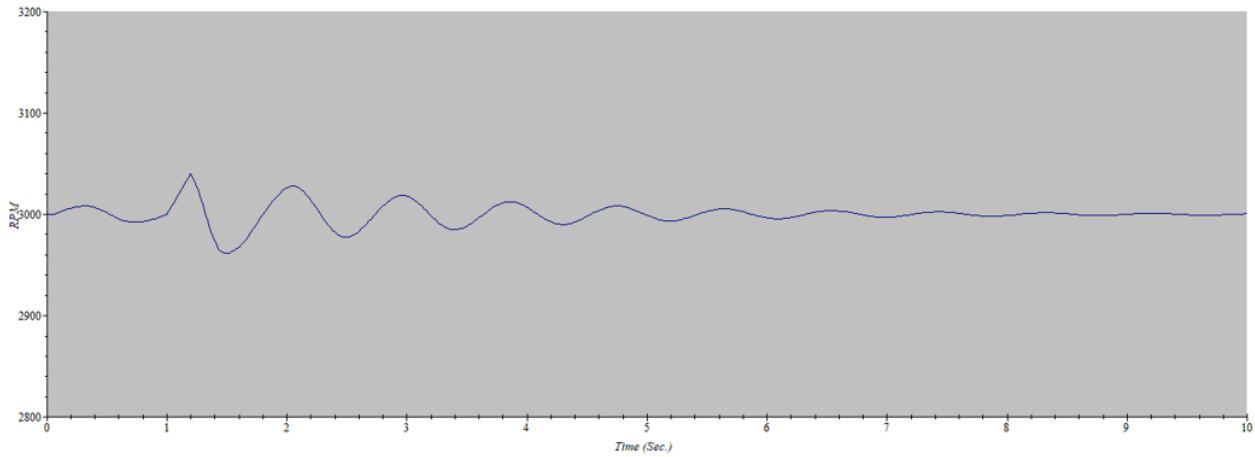
Fig. 4.24: A plot of generator speed versus time for a 83 MW machine

4.5 Calculation of the CCA and CCT using the EAC

The critical clearing angle and critical clearing time are calculated from the data obtained after performing power flow and transient stability analysis for Figs. 4.13 and 4.15. The data obtained are captured in Table 4.3. Two cases will be considered, one involving operations at 75 MW and the other at 83 MW.

4.5.1 Case 1: Generator operation at 75 MW, 0.85 lagging p.f.

Using the values in table 4.3, the critical clearing angle and critical clearing time are calculated as

$$\delta_c = \cos^{-1}\left[\frac{P_m}{P_{max}}(\pi - 2\delta_0) - (\cos\delta_0)\right]$$

56

P_{max} = 437.0629 MW; P_m = 75MW; δ_0 = 9.88° or 0.1724 radians

$\delta_c = \cos^{-1}\left[\frac{75}{437.0629}(\pi - 2 \times 0.1724) - (\cos 0.1724)\right]$ = 2.1005 radians; δ_c = 120.35°;

$\delta_{max} = \pi - \delta_0 = 180° - 9.88° = 170.12°$

Critical time t_c

$t_c = \sqrt{\frac{2H(\delta_c - \delta_0)}{P_{m,pu}\pi f}}$ seconds ; H = 3.585; P_m = 75MW; δ_0 = 9.88° or 0.1724 radians;

δ_c = 120.35° or 2.1005 radians; f = 50Hz;

$$t_c = \sqrt{\frac{2 \times 3.385(2.1005 - 0.1724)}{1 \times \pi \times 50}} = 0.28826s \text{ or } 288.26ms$$

4.5.2   Case 2: Generator operations at 83 MW, 0.95 lagging p.f.

Similarly using the information from Table 4.3, we have

critical clearing angle, $\delta_c = \cos^{-1}\left[\frac{P_m}{P_{max}}(\pi - 2\delta_0) - (\cos\delta_0)\right]$; δ_0 = 13.58° = 0.2370 radians;

$\delta_c = \cos^{-1}\left[\frac{83.6}{353.4887}(\pi - 2 \times 0.2370) - (\cos 0.2370)\right]$ = 1.9189 radians; δ_c = 109.75°

$$\delta_{max} = \pi - \delta_0 = 180° - 13.58° = 166.42°$$

critical clearing time, $t_c = \sqrt{\frac{2H(\delta_c - \delta_0)}{P_{m,pu}\pi f}}$ seconds.

$$t_c = \sqrt{\frac{2 \times 3.385(1.9189 - 0.2370)}{1 \times \pi \times 50}} = 0.26923s \text{ or } 269.24ms$$

From the calculations carried out, the value of the critical clearing angle for a machine operating at 75 MW, 0.85 lagging p.f., is higher than that of the machine operating at 83 MW, 0.95 lagging p.f., which translates to lower stability limits for the latter. This is proved by the maximum rotor angle for the individual machines; the maximum rotor angle is the angle a synchronous machine can attain before losing synchronism. Also, the critical clearing time is lower for the larger machine, implying that the fault should be cleared much faster to prevent the machine from becoming unstable.

Table 4.3: Data obtained from power flow simulation

NO.	Parameter	75MW 0.85 lagging p.f.	83MW 0.95 lagging p.f.
1	Mechanical Power (MW)	75	83.60
2	Mechanical Power (p.u)	1	1
3	Electrical Power (Steady State-MW)	75	75
4	Electrical Power Max (MW) Pre-Fault (Max)	437.0629	353.4887
5	Electrical Power (p.u) Pre-Fault (Max)	5.8275	4.2589
6	Electrical Power (MW) During Fault (Max)	0	0
7	Electrical Power (p.u) During Fault (Max)	0	0
8	Electrical Power (MW) Post Fault (Max)	437.0629	352.7426
9	Electrical Power (p.u) Post-Fault (Max)	5.8275	4.2589
10	Initial Rotor Angle (degrees)	9.88	13.58
11	Initial Rotor Angle (Radians)	0.1724	0.2370
12	Synchronous Speed (Rad/s), $\omega_s = 2\pi f$	314.1593	314.1593
13	$\sin\delta$	0.1716	0.2348
14	Frequency (HZ)	50	50

The summary of the EAC calculations is contained in Table 4.4.

Table 4.4: The results from the EAC calculations

NO.	Output (MW)	Operating Angle, δ_0 (deg.)	Max. Rotor Angle, δ_{max} (deg.)	Critical Angle, (δ_c) (deg.)	Critical Clearing Time (t_{cr}) (ms)
1	75	9.88	170.12	120.35	288.26
2	83	13.58	166.42	109.75	269.24

4.6 Computation of the CCA and CCT using modified Euler method

A solution to the transient stability problem can also be achieved using the numerical integration method. This section presents the application of the Modified Euler Method (MEM) to solving power system problems. The outcomes of the MEM are the CCA and the CCT. Reviewing the swing equation in (2.57),

$$\frac{d^2\delta}{dt^2} = \frac{\omega_0}{2H}(P_m - P_e),$$

This equation can be solved using the MEM; given that the equation is in second-order form, it can be transformed into two first-order differential equations as in (4.3) and (4.4) [31].

$$\frac{d\delta(t)}{dt} = \omega(t) - \omega_{syn} \tag{4.3}$$

$$\frac{d\omega(t)}{dt} = \frac{P_{mp.u.}(t) - P_{ep.u.}(t)\omega_{syn}}{2H\omega_{p.u.}(t)} \tag{4.4}$$

Applying the Euler method,

$$\widetilde{\delta_k} = \delta_k + \left(\frac{d\delta}{dt}\right)_k h \tag{4.5}$$

$$\widetilde{\omega_k} = \omega_k + \left(\frac{d\omega}{dt}\right)_k h \tag{4.6}$$

$$\left(\frac{d\widetilde{\delta}}{dt}\right)_k = \widetilde{\omega_k} - \omega_{syn} \tag{4.7}$$

$$\left(\frac{d\widetilde{\omega}}{dt}\right)_k = \frac{(P_{mp.u.k} - P_{ep.u.k})}{2H\widetilde{\omega}_{p.u.k}} \tag{4.8}$$

$$\delta_{k+1} = \delta_k + \frac{\left(\frac{d\delta}{dt}\right)_k + \left(\frac{d\widetilde{\delta}}{dt}\right)_k}{2} h \tag{4.9}$$

$$\omega_{k+1} = \delta_k + \frac{\left(\frac{d\omega}{dt}\right)_k + \left(\frac{d\widetilde{\omega}}{dt}\right)_k}{2} h \tag{4.10}$$

Where $t_k = t_0 + hk$ $(k = 0,1,2, \dots, \left[\frac{T}{h}\right]), h = t_{k+1} - t_k$

4.6.1   Implementing Euler method using spreadsheets

As given in the article [31], the Euler method can be alternatively implemented using Microsoft Excel spreadsheets. This work adopted this approach to eliminate the costs associated with commercial software. Equations (4.3–4.10) are transformed into Excel formulas in Table 4.5 [31]. The approach involves three stages: keying-in, computation, and graphical sections.

4.6.1.1 Keying-In section

Fig. 4.25 [31] shows section cells ranging from A1:F11 that contain preliminary values obtained from power flow in Figs. 4.10 and 4.12. Time to clear the fault is varied until stability is lost.

4.6.1.2 Computation section

Fig. 4.23 [31] shows section cells ranging from AI13:I114. Cell range A13:I13 contains the labels of the quantities that are computed, and A14:I14 contains initial values at zero time. Cells A15:I15 implement equations (4.2-4.10). The rest of the rows are replicas of A15:I15.

Table 4.5: The MEM Excel Formulas

Cell	Excel Formula	Description
A14	0	Initial time t_0. This is the instant at which the fault occurs; normally t_0 is set to zero.
B14	=D6	Copy the initial (pre-fault) power angle δ from cell D6.
C14	=D8	Copy the initial (pre-fault) generator (synchronous) speed ω from cell D8.
D14	=C14-$D$8	Generator relative speed at time step k, $\left(\frac{d\delta}{dt}\right)_k$, given by equation (4.3).
E14	=IF(A14>=$D$10,($D$2)-$D$5*SIN(B14))*$D$8^2/(2*$D$9*C14),($D$2-$D$4*SIN(B14))*$D$8^2/(2*$D$9*C14)	Generator acceleration at time step k, $\left(\frac{d\omega}{dt}\right)_k$, given by equation (4.4). The conditional IF is used to check whether the fault has been cleared or not so that the correct values of p_{e2} or p_{e3} is substituted in equation (4.4).
F14	=B14+D14*$D$11	Intermediate value of power angle at time step k, $\widetilde{\delta_k}$, given by equation (4.5).
G14	C14+E14*$D$11	Intermediate value of generator relative speed at time step k, $\widetilde{\omega_k}$, given by equation (4.6).
H14	=G14-$D$8	Slope correction for generator relative speed at time step k, $\left(\frac{d\widetilde{\delta}}{dt}\right)_k$, given by equation (4.7).
I14	=IF(A14>=$D$10,($D$2)-$D$5*SIN(F14))*$D$8^2/(2*$D$9*G14),($D$2-$D$4*SIN(F14))*$D$8^2/(2*$D$9*G14)	Slope correction for generator acceleration at time step k, $\left(\frac{d\widetilde{\omega}}{dt}\right)_k$, given by equation (4.8). IF is used to check whether the fault has been cleared or not so that the correct value of p_{e2} or p_{e3} is substituted in equation (4.8).
A15	=A14+$D$11	Updated value of time for current iteration. The time resolution is determined by the step size in cell D11.
B15	=B14+((D14+H14)/2)*$D$11	Updated power angle δ computed from equation (4.9).
C15	=C14+((E14+I14)/2)*$D$11	Updated generator relative speed ω computed from equation (4.10).
D15:I15	Various	Copies of formulas in cell range D14:I14
A16:I114	Various	Copies of formulas in cell range A14:I15

	A	B	C	D	E	F	G	H	I	J
1	Transient Stability Example									
2	Mechanical Power =			1	p.u.	% From power flow calculations				
3	Pre-fault maximum power (P_1max) =			4.2589	p.u.	% From power flow calculations				
4	During fault maximum power (P_2max) =			0	p.u.	% From power flow calculations				
5	Post-fault maximum power (P_3max)=			4.2589	p.u.	% From power flow calculations				
6	Initial (pre-fault) power angle (delta_0)			0.2370	rad	% From power flow calculations				
7	Frequency (f) =			50	HZ	%Frequency to be changed				
8	Synchronous speed (omega_s) =			314.1593	rad/s	%omega_s=2*pi*f				
9	Machine inertia constant (H)			3.385	p.u. -s	%inertia constant may be changed				
10	Clearance time (t_cl)			0.27	s	%fault clearance time may be changed				
11	Step size (Delta t)			0.01	s	%Time step for numerical methodnmay be changed				

Fig. 4.25: MEM keying-in section of spreadsheets for transient stability analysis

	A	B	C	D	E	F	G	H	I	J
32	0.18	0.9176	322.4039	8.2446	45.2179	1.0001	322.8561	8.6968	45.1546	57.30082624
33	0.19	1.0023	322.8558	8.6965	45.1547	1.0893	323.3074	9.1481	45.0916	62.41309970
34	0.20	1.0916	323.3070	9.1477	45.0916	1.1830	323.7580	9.5987	45.0288	67.78372832
35	0.21	1.1853	323.7576	9.5983	45.0289	1.2813	324.2079	10.0486	44.9663	73.41235255
36	0.22	1.2835	324.2076	10.0483	44.9664	1.3840	324.6573	10.4980	44.9041	79.29861429
37	0.23	1.3863	324.6570	10.4977	44.9041	1.4912	325.1060	10.9467	44.8421	85.44215697
38	0.24	1.4935	325.1057	10.9464	44.8422	1.6030	325.5541	11.3948	44.7804	91.84262548
39	0.25	1.6052	325.5538	11.3945	44.7804	1.7191	326.0016	11.8423	44.7189	98.49966617
40	0.26	1.7214	326.0013	11.8420	44.7190	1.8398	326.4485	12.2892	44.6577	105.4129268
41	0.27	1.8420	326.4482	12.2889	44.6578	1.9649	326.8948	12.7355	44.5967	112.5820568
42	0.28	1.9672	326.8945	12.7352	44.5968	2.0945	327.3404	13.1811	44.5360	120.0067067
43	0.29	2.0967	327.3401	13.1808	-179.9218	2.2286	325.5409	11.3816	-161.7396	127.6865286
44	0.30	2.2196	325.6318	11.4725	-163.1209	2.3343	324.0006	9.8413	-144.4331	133.7443645
45	0.31	2.3261	324.0941	9.9348	-145.8634	2.4255	322.6354	8.4761	-127.6736	138.969254
46	0.32	2.4182	322.7264	8.5671	-129.0813	2.5038	321.4356	7.2763	-112.0068	143.4599569
47	0.33	2.4974	321.5209	7.3616	-113.3439	2.5710	320.3875	6.2282	-97.7194	147.3080704
48	0.34	2.5653	320.4656	6.3063	-98.9577	2.6284	319.4760	5.3167	-84.9237	150.5966163
49	0.35	2.6235	319.5462	5.3869	-86.0495	2.6773	318.6857	4.5264	-73.6207	153.3995944
50	0.36	2.6730	318.7479	4.5886	-74.6306	2.7189	318.0016	3.8423	-63.7453	155.7821305
51	0.37	2.7152	318.0560	3.8967	-64.6426	2.7541	317.4096	3.2503	-55.1969	157.8009616
52	0.38	2.7509	317.4568	3.2975	-55.9890	2.7839	316.8969	2.7376	-47.8599	159.5050912
53	0.39	2.7811	316.9375	2.7782	-48.5563	2.8089	316.4520	2.2927	-41.6161	160.9365061

Fig. 4.26: Implementation of the MEM using spreadsheets

4.6.1.3 Graphical section

Figs. 4.27 and 4.28 show conditions of stability and instability, respectively, for the 75 MW machine. In the first case, the fault is cleared at the CCT of 290 ms, corresponding to the CCA of 127.69 degrees, and the later indicates a fault is cleared in time longer than the CCT, i.e., 300 ms.

Fig. 4.27: A plot of a rotor angle versus time for a stable machine at 75 MW, CCT = 290 ms

Fig. 4.28: A plot of a rotor angle versus time for an unstable machine at 75 MW, CT delayed to 300 ms

Figs. 4.29 and 4.30 [32] show a typical example of transient stability analysis using the modified Euler method for a stable and an unstable system, respectively. In the first graph, the fault is cleared in a shorter time than the CCT, and in the latter, fault clearance is delayed beyond the CCT, thus leading to system instability.
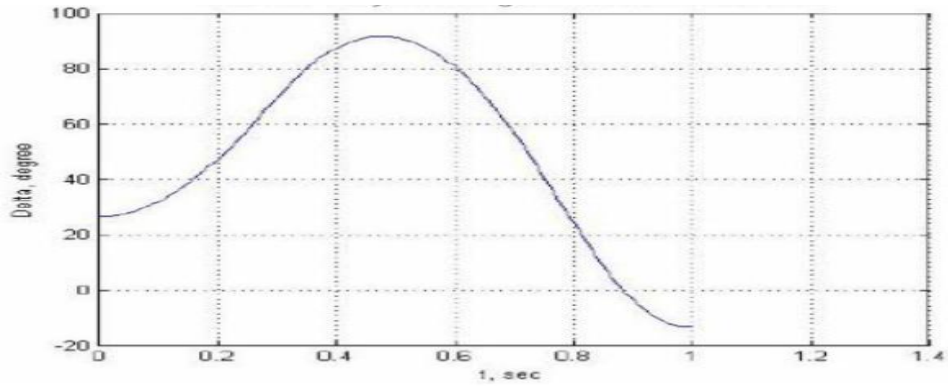
Fig. 4.29: A typical case of EM for a stable system
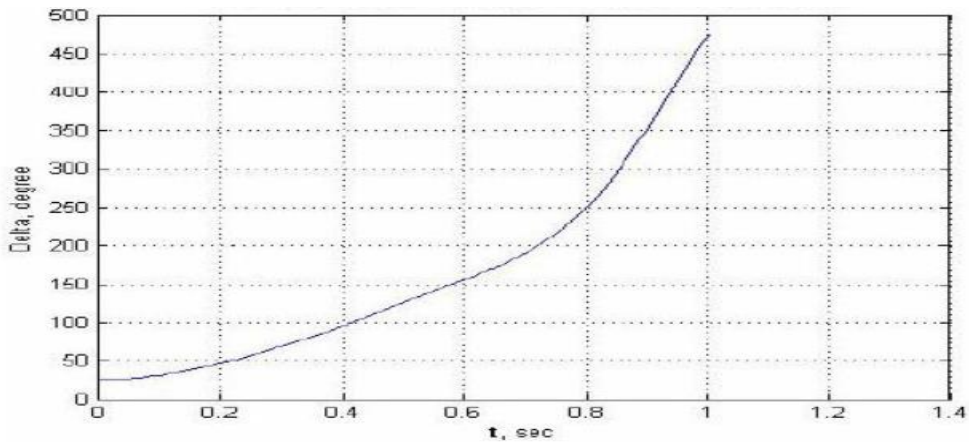
Fig. 4.30: A typical case of EM an Unstable system

Figs. 4.31 and 4.32 show conditions of stability and instability, respectively, for the 83 MW machine. In the first case, the fault is cleared at the CCT of 270 ms, corresponding to the CCA of 109.24 degrees, and the later indicates a fault is cleared in time longer than the CCT, i.e., 280 ms.
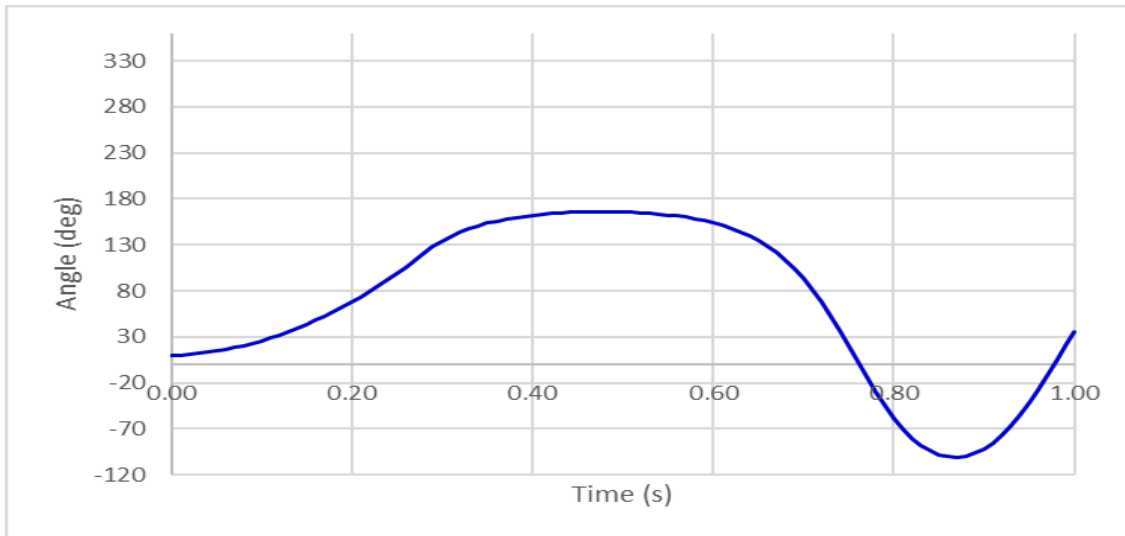
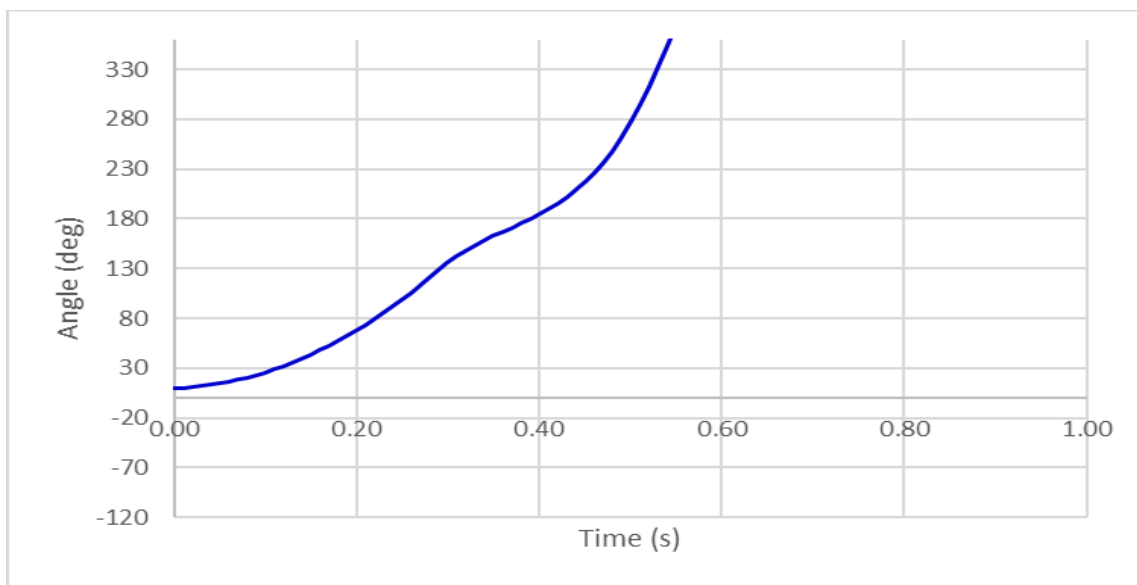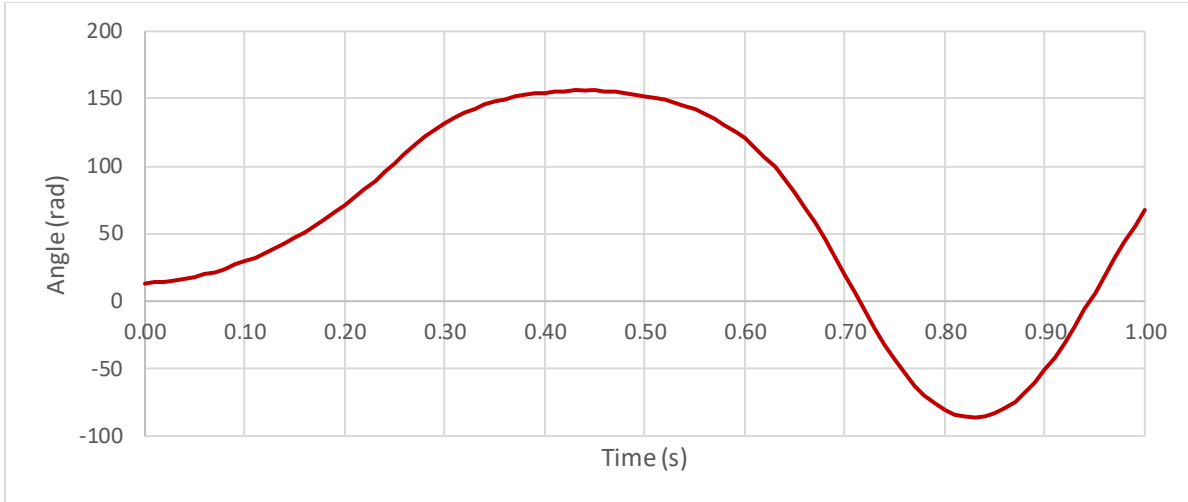*Fig.4.31: A plot a rotor angle versus time for a stable machine at 83MW, CCT = 270 ms*
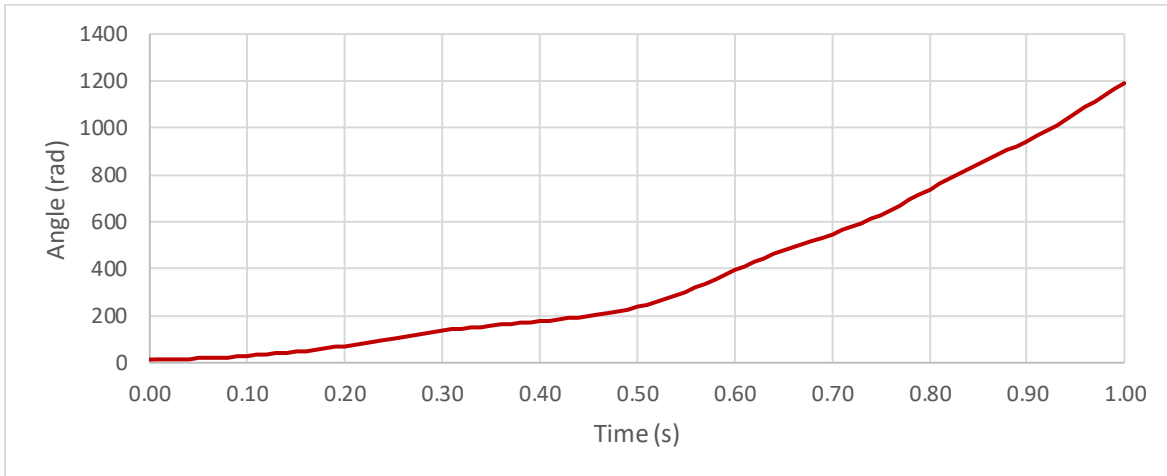
Fig.4.32: A plot a rotor angle versus time for an unstable machine at 83MW, CT delayed to 280 ms

4.7 Validation of the results

To confirm that the EAC results obtained from the research are meaningful, the modified Euler method (MEM) was adopted as a check method. MEM is a numerical integration method that gives an approximate solution as compared to the EAC method, which uses analytical techniques. In this case, EAC is treated as more accurate and therefore forms the reference. Table 4.6 compares the results from the two methods. The deviations were less than 10%, which is acceptable in any experiment. Therefore, the thesis results are valid.

Table 4.6: Comparison of the results between the EAC and MEM

Rating (MW)	Critical Angle (deg.)		Critical Clearance Time (ms)		Error in Angle		Error in Time	
	EAC	Euler	EAC	Euler	deg.	%	ms	%
75	120.35	127.69	288.26	290.00	7.34	6.10	1.74	0.60
83	109.75	109.24	269.24	270.00	-0.51	-0.46	0.76	0.28

4.8 Chapter conclusion

The chapter analyzes the results generated by the system models. The analyzed results are presented in both graphical and tabular formats. The stability analyses were performed using the EAC and MEM. The results obtained from the two methods were comparable with small deviations.

CHAPTER 5: CONCLUSIONS AND RECOMMENDATIONS

5.1 Conclusions

The research carried out to determine the changes in the transient stability behavior when a generator of 75 MW is uprated to 85 MW at the Olkaria IV geothermal power plant in Kenya showed that the latter would be less stable when compared to the former. This is attributed to the reduced excitation, which plays a vital role in maintaining system stability. The results from the applied method, the equal area criterion, showed that the critical clearing angle would decrease from 120.35 degrees to 109.24 degrees and the critical clearing time would decrease from 288.26 milliseconds to 269.24 milliseconds. This is likely to pose stability problems unless measures are put in place to correct the situation. The comparison of results between the EAC and MEM yielded acceptable deviations ranging from -0.4% to 6.10% and 0.28% to 0.60% for the critical clearing angle and critical clearing time, respectively, thus making them valid.

5.2 Contributions

This work is a contribution to the knowledge of geothermal power generation in Kenya, the role played by the geothermal machines in system stability, and the general synchronous machine behavior when subjected to system disturbances. The knowledge can be applied in both the industrial and academic fields. The sources of information presented in the thesis can form part of the secondary sources for those planning to pursue research in the same field. Also, the information contained in this thesis will be useful to the generation and transmission companies when it comes to the optimization of system parameters.

5.3 Recommendations

The thesis recommends that the result be adopted by revising the relay protection settings so that the electrical faults are cleared in appropriate time to ensure synchronism is maintained in the event the machine is uprated. Another recommendation is to design alternative voltage control methods such as capacitor banks and static synchronous compensator (STATCOM) devices to compensate for the reduction in generator reactive power caused by the uprate. Finally, the thesis recommends other transient stability methods, such as Runge-Kutta.

REFERENCES

[1] S. K. Mahapatro, "Transient Stability Analysis in Interconnected Power System for power Quality Improvement," *IJERT* vol. 2, Feb. 2013.

[2] P. R. Sharma and N. Hooda, "Transient Stability Analysis of Power System Using Matlab," *IJESRT*, Sep. 2012.

[3] A. Abbas *et al*, "Power System Transient Stability Case Study: A Power Sub-Station Plant in Sudan," *ISJ,* June 2014.

[4] J. U. Agber *et al*, "Effects of Power System Parameters on Transient Stability Studies," *AJER* vol. 2, pp 87-94, 2015.

[5] H. saadat, "Stability," *in Power System Analysis,* McGraw-Hill college, 1998, ch.11 p. 460

[6] J. J. Grainger and W. D. Stevenson, "Power System Stability," *in Power System Stability Analysis,* 1994, ch.16 p. 695.

[7] D. Abakar *et al*, "Transient Stability Analysis of the Multimachine Power System Using Etap-Software," *IJEEE* vol. 6, pp 1-12, 2020.

[8] P. Kundur, "Introduction to the power system stability problem," *in Power System Stability and Control,* McGraw Hill Education India, 1994, ch. 2 pp. 17-27.

[9] M. V. Rao, "Power System Stability" Electrical & Electronics Eng. Dept. University of JNTUA college of engineering, Kalikiri Chittoor District, A P India.

[10] A.H. Prajapatis and P.Mihir, "Basic Concept of Power System Stabilizer for Power System Stability and Comparison of Different Design Methods," IJTRE journal, vol.1, issue 11, p 1398, July 2014.

[11] C. A. Gross, "A Method for Determining Transient Stability in Power Systems" Doctoral dissertations, Elect. & computer Eng. Dept. University of Missouri, USA 1969.

[12] EPRA Report, "Least Cost Power Development Plant 2021-2030," April 2021.

[13] P. M. Anderson, A. A. Fouad, "Power System Stability," *in Power System Control and Stability,* Wiley 2002, p 4.

[14] H. Himadri *et al*, " Transient Stability Analysis of Syncronous Generator in Power System ," *IRJET* vol. 7, June 2020.

[15] J. Machowski, J. Bialek, Dr. J. Bumby, "Introduction to power system," *in Power System Dynamics Stability and Control,* Wiley, 2008, p 9.

[16] P. S. Murty, "Power System Stability" *in System Stability Analysis,* BH Publications, 2017, Ch. 13 pp. 365-371.

[17] M. V. Rao. (2011). Power System Stability.

[18] J. Sutter and J. Maleche, "Analysis of Power System Transient Stability Due to increases Integration of Geothermal Power," Proceedings, Thirty-Ninth Workshop on Geothermal Reservoir Engineering Stanford University, Stanford, California, Feb. 24-26, 2014, p 2.

[19] H. Al Marhoon, "Practical Method for Power System Transient stability and Security" MSc. Elect. Eng. Dept. University of New Orleans, France 2011.

[20] L. A. A. Lopez, "Modelling and Stability Analysis of Berlin Geothermal Power in El Salvador," MSc dissertation, dept. Eng. United Nation University, 2013.

[21] S. Padhi and B. P. Mishra, "Representation of Transient Stability for Power System Dynamics Using Numerical Integration Method and Damping," *IJAIEM* vol. 4, Feb. 2015.

[22] D. K. Chaturvedi, "System Modeling," *in Modeling and Simulation of System using MATLAB and Simulink*, CRC press, New York 2010, p 32.

[23] D. P. Kothari, "Synchronous Machine", *in Electric Machines,* Fourth Edition McGraw-Hill Higher Education New Delhi, 2010, p. 497.

[24] Dr. S. Ibrahim, "II Synchronous Generators," unpublished.

[25] P. Kundur, "Synchronous Machine theory and modelling," *in Power System Stability and Control,* McGraw Hill Education India, 1994, ch.3 pp. 128 – 135.

[26] R. K. Padiyar, "Review of the Classical Methods," *in Power System Dynamics Stability and Control,* BS Publications, 2008, pp. 9-10.

[27] P. Kundur, "Transient stability," *in Power System Stability and Control,* McGraw Hill Education India, 1994, ch.3 pp. 830 – 832.

[28] P. S. Murty, "Power System Stability" *in System Stability Analysis,* BH Publications, 2017, Ch. 13 pp. 365-371.

[29] S. Sivasubramani, "Power System Dynamics and Control" Dept. of Electrical Engineering, Indian Institute of Technology (www.iitp.ac.in/~siva).

[30] P. Kundur, "Small Signal Stability," *in Power System Stability and Control,* McGraw Hill Education India, 1994, ch.12 p. 706.

[31] Turabo University Online. (2010). Computer-Based Approach to the Analysis of Transient Stability of Power Systems.

[32] S. Padhi and B. P. Mishra, "Numerical Method Based Single Machine Analysis for Transient Stability," *IJATAE* vol. 2, p331, Feb. 2014.

APPENDICES

Appendix A: Published Papers

The following conference papers have been published by the author:

1) "*Improvement of small-signal stability by tuning PSS parameters for geothermal machines in Kenya" was* published on 3rd October 2022 on the IEEE Xplore website. The paper suggested ways to mitigate the effects of small signal instabilities in the Kenyan Grid network by the installation and optimal tuning of power system stabilizers domiciled in generator automatic voltage regulators (AVR).

2) "*Performance Analysis for Numerical Relays in Implementing Loss of Field in Generator Protection*," that was also published on 3rd October 2022 on the IEEE Xplore website. The paper sought to address relay maloperation due to improper relay configuration and calculation of the protection setting. The paper suggested ways of calculating the loss of field protection settings for synchronous generators.

Appendix B: System data

Table B1: Olkaria IV generator data

Generator type	Round Rotor
MW/MVA rating of the machines	75.267/88.55
Max output (MW)	75
Max (MVAR)	45
Min (MVAR)	-25
Lagging PF limit	0.8
Leading PF limit	0.95
Rated output PF	0.85
Rated Speed at 50Hz output, RPM	3000
Direct axis synchronous reactance, X_d	189%
Direct axis transient reactance, X'_d	27%
Direct axis sub-transient reactance, X''_d	15%
Zero Sequence Reactance, X_0	9.5%
Leakage reactance, X_1	12.5%
Positive Sequence, R_1	0.4%
Transient no-load time constant, $T'do$	5.923
Sub-Transient no-load Time Constant, $T''do$	0.037
Transient short circuit time constant, Td'	7.8
Sub - transient short circuit time constant, Td"	0.06
Quadrature axis transient no-load time Constant, $T'qo$	0.54
Quadrature axis sub-transient no-load time constant, $T''qo$	0.07
Inertia constant, H	3.385

Table B2: Turbine data

Controller lag in seconds	T_1	0 sec
Controller lead compensation in seconds	T_2	0 sec
Governor lag in seconds	T_3	0.02 sec
Delay due to steam inlet volumes associated in steam chest and inlet piping.	T_4	0.42 sec
Gain (CV regulation 5%)	K_1	20
Upper power limit	P_{max}	1.1
Lower power limit	P_{min}	0

Table B3: Exciter data

AVR power stage gain	K_a	640
AVR power stage Time Constant	T_a	0.03 sec
AVR positive ceiling voltage	V_{max}	13.24 V
AVR negative ceiling voltage	V_{min}	(-)10.79
Rectifier regulation	K_c	0.174
Demagnetizing constant	K_d	0.353
Exciter field proportional Constant	K_e	1
Exciter Time Constant	T_e	1.07 sec
Saturation Coefficient	E_1	6.57
Saturation Coefficient	E_2	4.93

Table B4: Power transformer data

Generator side voltage	kV	11
Transmission side voltage	kV	220
Rating	MVA	90
Impedance	@ ONAN	12%
Tap range		+10% to -10%
Automatic/Manual		Automatic
Number of Taps		19

Table B5: Power transformer data

Conductor Type	Voltage	R1(Ω/km)	X1(Ω/km)	B1(S/km)	I (amps)	S(MVA)
220_CANARY	220	0.07649	0.44	2.63E-06	720	274

Conductor cross-sectional area - 515.16mm^2

Conductor diameter - 29.52mm^2
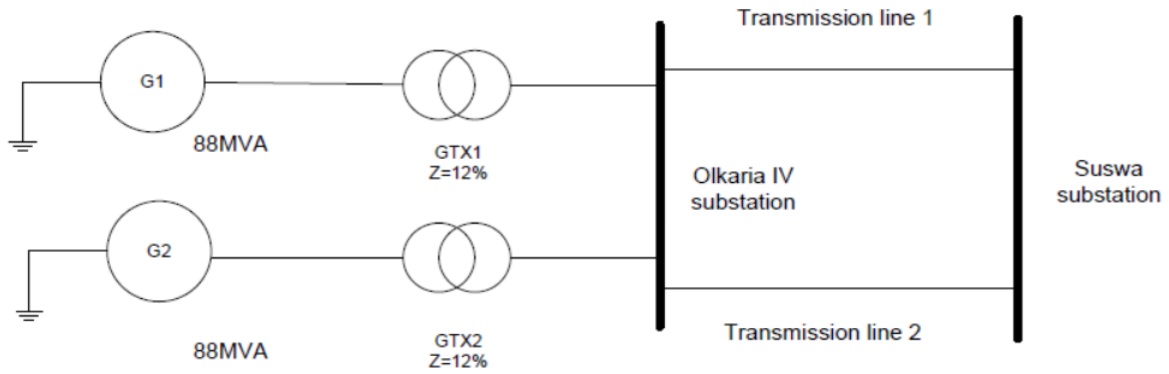
Length of the line – 20km

Fig. B1: System model

Appendix C: ETAP functions

C1: 75MW machine

Harmonic	Protection	Reliability	Fuel Cost	Time Domain	O & M	Remarks	Comment
Info	Rating	Capability	Imp/Model	Grounding	Inertia	Exciter	Governor	PSS

11 kV   75 MW   Voltage Control

Rating

MW	kV	% PF	MVA	% Eff.	Poles
75	11	85	88.235	95	2

% of Bus Nom. kV	FLA	RPM
100	4631	3000

	Gen. Category	% V	Angle	MW	Mvar	% PF	Qmax	Qmin
1	Design	100		75			46.481	0
2	Normal	100		0			72.918	0
3	Shutdown	100		0			72.918	0
4	Emergency	100		0			72.918	0

Prime Mover Rating

Continuous		Peak	
HP	MW	HP	MW
100577	75	100577	75

Mvar Limits

◉ Capability Curve
○ User-Defined

Peak Mvar
46.481

Operating Values

% V	Vangle	MW	Mvar
100	6.8	75	0.333

Gen1

OK   Cancel

C1: 83MW machine

Harmonic	Protection	Reliability	Fuel Cost	Time Domain	O & M	Remarks	Comment
Info	Rating	Capability	Imp/Model	Grounding	Inertia	Exciter	Governor	PSS

11 kV   83.2 MW   Voltage Control

Rating

MW	kV	% PF	MVA	% Eff.	Poles
83.2	11	95	87.579	95	2

% of Bus Nom. kV	FLA	RPM
100	4597	3000

	Gen. Category	% V	Angle	MW	Mvar	% PF	Qmax	Qmin
▶1	Design	100		83			27.572	0
2	Normal	100		0			64.8	0
3	Shutdown	100		0			64.8	0
4	Emergency	100		0			64.8	0

Prime Mover Rating

Continuous		Peak	
HP	MW	HP	MW
111305	83	111305	83

Mvar Limits

◯ Capability Curve

◉ User-Defined

Peak Mvar: 27

Operating Values

% V	Vangle	MW	Mvar
100	6.8	83	0.333

Gen1   OK   Cancel

74

Appendix D: Similarity Index Report